AFRL-AFOSR-VA-TR-2020-0106

Distributed Radar Imaging in Contested Environments

Birsen Yazici
RENSSELAER POLYTECHNIC INST TROY NY

07/01/2020
Final Report

Air Force Research Laboratory
AF Office Of Scientific Research (AFOSR)/ RTB1
Arlington, Virginia 22203
Air Force Materiel Command

DISTRIBUTION A: Distribution approved for public release.

REPORT DOCUMENTATION PAGE

Form Approved
OMB No. 0704-0188

1. REPORT DATE *(DD-MM-YYYY)*	2. REPORT TYPE	3. DATES COVERED *(From - To)*
22-07-2020	Final Performance	01 Jul 2016 to 31 Oct 2019

4. TITLE AND SUBTITLE
Distributed Radar Imaging in Contested Environments

5a. CONTRACT NUMBER

5b. GRANT NUMBER
FA9550-16-1-0234

5c. PROGRAM ELEMENT NUMBER
61102F

6. AUTHOR(S)
Birsen Yazici

5d. PROJECT NUMBER

5e. TASK NUMBER

5f. WORK UNIT NUMBER

7. PERFORMING ORGANIZATION NAME(S) AND ADDRESS(ES)
RENSSELAER POLYTECHNIC INST TROY NY
100 8TH STREET
TROY, NY 12180 US

8. PERFORMING ORGANIZATION REPORT NUMBER

9. SPONSORING/MONITORING AGENCY NAME(S) AND ADDRESS(ES)
AF Office of Scientific Research
875 N. Randolph St. Room 3112
Arlington, VA 22203

10. SPONSOR/MONITOR'S ACRONYM(S)
AFRL/AFOSR RTB1

11. SPONSOR/MONITOR'S REPORT NUMBER(S)
AFRL-AFOSR-VA-TR-2020-0106

12. DISTRIBUTION/AVAILABILITY STATEMENT
A DISTRIBUTION UNLIMITED: PB Public Release

13. SUPPLEMENTARY NOTES

14. ABSTRACT
The goal of this research is to advance distributed radar imaging in contested and challenging environments. Contested environments are typically uncertain, complex and ambiguous areas where radar's capabilities are limited, denied or deceived. Both distributed active & passive radar provide important sensing capabilities in contested environments. The objectives of the project are organized along the following topics: i) Passive imaging of extended and moving targets. This aims to develop methods to overcome the limitations of widely used time or frequency difference of arrival based backprojection techniques. ii) Passive multi-static, polarimetric imaging. iii) Analysis of artifacts in SAR imagery. We quantify artifacts caused by phase errors such as unknown refractive index or ground topography.

15. SUBJECT TERMS
passive microwave sources

16. SECURITY CLASSIFICATION OF:			17. LIMITATION OF ABSTRACT	18. NUMBER OF PAGES	19a. NAME OF RESPONSIBLE PERSON
a. REPORT	b. ABSTRACT	c. THIS PAGE			NACHMAN, ARJE
Unclassified	Unclassified	Unclassified	UU		19b. TELEPHONE NUMBER *(Include area code)* 703-696-8427

Standard Form 298 (Rev. 8/98)
Prescribed by ANSI Std. Z39.18

AFOSR Grant FA9550-16-1-0234
Final Report

August 01, 2016 - October 31, 2019

Principal Investigator: Birsen Yazıcı

Department of Electrical, Computer and Systems Engineering
Rensselaer Polytechnic Institute
Troy, NY 12180
yazici@ecse.rpi.edu

June 30, 2020

Contents

Chapter 1

Project description

1.1 Objectives

The overall goal of this research project is to advance the distributed radar imaging in contested and challenging environments. Contested environments are typically uncertain, complex and ambiguous areas where radars capabilities are limited, denied or deceived. Both distributed active and passive radar provide important sensing capabilities in contested environments. Passive radar also offers efficient use of RF spectrum in congested environments.

The objectives of the project are organized along the following topics: *i*) Passive imaging of extended and moving targets - This research aims to develop methods to overcome the limitations of widely used time or frequency difference of arrival based backprojection techniques. Our approach focuses on convex and non-convex optimization methods, computational efficiency and performance analysis in the presence of uncertainties and limited spectral data. *ii*) Passive polarimetric imaging - We investigate the value of polarimetric diversity in passive detection and imaging. The methods we develop range from filtered-backprojection to statistical methods and optimization based approaches that take advantage of underlying tensorial structures in our polarimetric model. *iii*) Analysis to algorithms - We develop quantitatively analysis of certain artifacts observed in SAR imagery. These include analysis of artifacts due to antenna trajectory errors, moving targets, non-flat or unknown ground topography, and unknown refractive index of background propagation medium. Our analysis shows that these artifacts contain valuable information. We develop methods to extract this information, specifically for motion estimation from smearing analysis and height estimation from layover

analysis.

In addition to the objectives above, we also explore the machine learning, specifically deep learning and optimization methods in addressing the problems of distributed radar imaging.

The project included a sub-task conducted by Prof. John Christian of Rensselaer Polytechnic Institute. The final report on this sub-task is included in Appendix A.

1.2 Personnel Supported

1.2.1 Faculty

- Birsen Yazıcı (Principal Investigator)
- John Christian (Investigator for a sub-task)

1.2.2 Graduate students supported

The project provided partial support to the following graduate students:

- Il-Young Son (US Citizen)
- Eric Mason (US Citizen)
- Bariscan Yonel (Citizen of Republic of Turkey)
- Avi Ryderman (US Citizen)
- Devin Renshaw (US Citizen)

Additionally, the PI hired the following students: Samia Kazemi (Citizen of Bangladesh) in January 2018. She is working on a sonar imaging and machine learning project and supported by the Office of Naval Research. Sean Thammakhoune hired in January 2019 (US Citizen). Sean is supported by AFOSR and is working on blind deconvolution and ground moving target imaging. Airas Akthar (Citizen of Pakistan) hired in June 2019. She is supported by National Science Foundation and is working on exact interferometric inversion with a priori information. Matthew Caulfield (US Citizen) hired in Fall 2019. Matthew is currently a teaching assistant. Once he successfully passes his doctoral qualifying exam, he will be supported by AFOSR. His thesis is on optimization methods and

autofocus problem. Avi Ryderman whom I hired in Fall 2018, dropped out of the PhD program in Spring 2019 and is no longer with Rensselaer. He was hired by Raytheon to work on radar signal processing.

Devin Renshaw is a graduate student in J. Christian's research program who worked on the subtask.

1.2.3 Thesis

The students who are partly supported by the AFOSR grant have completed or are working on the following PhD thesis topics:

- Eric Mason – Passive Radar Detection and Imaging using Low-Rank Matrix Recovery. Graduated in December 2017. Currently with Naval Research Laboratory, Washington DC.

- Il-Young Son – Multistatic Polarimetric Passive Radar Imaging. Graduated in December 2018. Working as a data scientist for NBA.

- Bariscan Yonel – A Theory of Exact Interferometric Inversion for Wave-Based Imaging. Expected graduation in Fall 2020.

Chapter 2

Current Status of Effort

2.1 Collaborations

- My former student, Eric Mason, defended his PhD thesis successfully in August 2017 and joined Naval Research Laboratory (NRL), Washington DC in Fall 2017. Eric spent the summer of 2016 as an intern in Air Force Research Laboratory (AFRL), Wright-Patterson, Automatic Target Recognition (ATR) Center. We were also fortunate to arrange tuition and stipend support for Eric from Ed Zelnio's ATR Center for Fall 2016 and Spring 2017. Eric and I continue to collaborate on a number of topics related to his thesis and beyond. Specifically, I consulted Eric on group theory as certain operators that arise in radar signal processing are group representations. We also continue to collaborate on machine learning for passive radar imaging. Specifically, Eric and my current PhD student Bariscan Yonel and I published an invited manuscript on deep learning and waveform estimation for passive Synthetic Aperture Radar (SAR) imaging to IET Radar, Sonar and Navigation Journal special issue. Other topics that Eric, Bariscan and I are collaborating involves passive SAR imaging from phaseless measurements and non-convex optimization methods for exact recovery of extended targets in passive SAR. Currently, we are drafting two journal papers on these topics. Eric appears to be doing very well at NRL, already leading several projects as a PI and looking to develop new ones. The management in NRL appears very happy to have Eric on board and are looking to hire more students from my research group.

- In Fall 2019, I hired a new graduate student Sean Thammakhoune. Sean

spent his first year learning the basics of radar and computational imaging. He spent the summer of 2019 at NRL working with Dr. Eric Mason. Sean is doing a remote internship with NRL in summer 2020. His thesis will be on moving target imaging using optimization and machine learning methods. NRL already expressed interest in hiring Sean upon his graduation. Sean cleared his doctoral qualifying exam in Fall 2019 and I started supporting him with our new AFOSR grant since January 2020.

- My PhD student Il-Young Son (US Citizen) completed his PhD thesis in Fall 2018. His thesis topic explores polarimetry for multi-static passive radar. Il-Young was a summer intern at AFRL in 2016 working on airborne polarimetric passive radar per Richard Albanese suggestion. Il-Young co-authored a journal paper on Doppler Synthetic Aperture Radar Interferometry, machine learning on passive radar and optimization for multi-static radar. NRL had planned on hiring Il-Young. However, security related technical problems prevented the planned hiring. Il-Young stayed with my research program for about half a year during which he completed a journal paper and secured a job as a data scientist in National Basketball Association.

- Starting Spring 2017, I have been supporting Bariscan Yonel to work on my AFOSR project. Bariscan has passed the PhD qualifying exam as a top student in the department. He is self-motivated and has extremely good analytic skills. Bariscan very quickly learned the basics of synthetic aperture imaging, analytic image reconstruction techniques and machine learning and optimization theory. Bariscan, Eric and I wrote two journal papers addressing synthetic aperture image reconstruction in machine learning framework. Specifically, we are looking into Deep Learning methods. Bariscan, Eric and I co-authored a number of conference papers on the topic. These papers drew significant attention and I was invited to write two journal articles on the topic, one for the IEEE Journal Special Topics on Machine Learning in RF Communication and Radar and another one for IET Journal on Radar, Sonar and Navigation special issue on high resolution passive radar imaging. In addition to Deep Learning approach to computational imaging problems, Bariscan, and I have also developed novel, provably good, computationally efficient, non-convex optimization methods for imaging with applications to passive radar and phaseless imaging. Thus far, Bariscan co-authored five high quality journal publications and we are cur-

rently working on two other manuscripts. Bariscan has strong analytic skills and ability to tackle fundamental theoretical problems. He has been collaborating with three other graduate students in my research group. Bariscan is planning to defend his thesis in early Fall 2020 and graduate in December 2020. He plans to look for an academic position in US.

- In January 2018, I hired Samia Kazemi as a graduate research assistant. Samia is funded by a Navy grant on sonar imaging and automatic target recognition. Samia has good analytic skills. She is very bright and hard working. She passed her PhD qualifying exam as the top student in the department. She took my radar imaging course in Spring 2018 and quickly built her background in computational imaging, radar and sonar. Samia, Bariscan and I are developing Deep Learning methods for mine detection and classification and sonar imaging in uncertain and dynamically changing ocean environments. These techniques have direct applicability to radar imaging and radar automatic target recognition (ATR).

- I hired a new graduate research assistant, Avi Ryderman (US Citizen), in Fall 2018 and started supporting Avi by my AFOSR grant. (Avi was admitted to RPI with good credentials. He graduated from University of California, Santa Barbara , CA with a BS degree in Electrical Engineering.) Unfortunately he could not maintain the minimum required grade point average at RPI and dropped out of the program in Spring 2019. Nevertheless, Avi secured a position at Raytheon as a radar engineer.

- I also arranged summer internship for Richard Chen, my former PhD student, at AFRL, ATR Center in 2016. Richard worked on learning the basics of SAR processing and pattern recognition algorithms. Unfortunately, Richard failed to pass the PhD qualifying exam in Fall 2016 and had to quit the PhD program at the end of 2016.

- We started collaborating with Prof. Piotr Samczynski of Warsaw University of Technology, Institute of Electronic Systems. Piotr is a young and a very productive researcher who has received Fred Nathanson Memorial Radar Award in 2017. Piotr's group has developed a high fidelity electromagnetic simulator and we are using this simulation platform to generate synthetic data for training and testing our machine learning algorithms.

- Prof. Yuejie Chi of Carnegie Mellon University and I started a collaboration on developing non-convex optimization methods for certain problems that

arise in passive radar and sensor networks. I brought the problem to Yuejie's attention and some of Yuejie's publications were very helpful in getting a good understanding of the problem. Since our initial discussion, my student Bariscan and I have developed the method fully. We plan to visit Yuejie or invite her to RPI to discuss further collaborations.

- Prof. Ilker Bayram of Istanbul Technical University visited my research group in Spring 2017. Prof. Bayram's area of expertise is convex optimization. Dr. Bayram, then my student Dr. Eric Mason and I co-authored a conference paper on weakly convex optimization for phaseless imaging. Additionally, Eric, Ilker and I co-authored a book chapter entitled "Optimization Methods for Synthetic Aperture Radar Imaging," published in Handbook of Convex Optimization Methods in Imaging Science by Springer-Verlag in 2018.

- I continued to collaborate with my former post-doctoral associate Dr. Ling Wang on theoretical aspects of radar imaging. Ling and I co-authored two journal papers and a number of conference papers.

- Dr. Xin Wang of Nanjing University visited my research group in Fall 2017. I encouraged Xin to work on some theoretical problems in computational wave based imaging. However, Xin did not seem to have the right orientation to tackle such problems. She instead worked on implementing iterative schemes for image reconstruction. Xin returned to her home institution in September 2018.

- I have mentored Daryl Osterloh of University of Dayton on radar imaging within IEEE AES Society professional networking and mentorship program. Daryl is a first year PhD student working on radar tomography with Dr. Michael Wicks.

- I arranged summer internships for a number of graduate students in defense industry. These students and some of the undergraduates who took my radar imaging course in Spring 2018 went on to work for defense companies.

Chapter 3

Interactions/Transitions

My students and I attended the conferences and meetings in US and Europe; presented our research and interacted with colleagues in other universities, AFRL researcher and researchers in industry.

3.1 Activities in 2016-2017

My students and I attended IEEE Radar Conference in Seattle, WA; SPIE Defense and Security Conference in Anaheim, CA; IEEE International Conference on Acoustics and Signal Processing, New Orleans and IEEE International Radar Symposium (IRS) Prague, Czech Republic. In these meetings, we presented the following papers:

1. I. Y. Son and B. Yazici, "Passive Polarimetric Reconstruction of Extended Dipole Targets," IEEE International Radar Symposium, Prague, Czech Republic, June 2017.

2. L. Wang and B. Yazici, "Height reconstruction using differential layover for SAR imagery," 2017 IEEE Radar Conference (RadarConf), Seattle, WA, 2017, pp. 0163 - 0168.

3. L. Wang and B. Yazici, "Effects of fluctuation in refractive index of atmosphere on synthetic aperture radar images," 2017 IEEE Radar Conference (RadarConf), Seattle, WA, 2017, pp. 0169 - 0174.

4. E. Mason, B. Yonel and B. Yazici, "Deep learning for radar," 2017 IEEE Radar Conference (RadarConf), Seattle, WA, 2017, pp. 1703-1708.

5. E. Mason, B. Yonel, B. Yazici, "Deep learning for SAR image formation," Proc. SPIE 10201, Algorithms for Synthetic Aperture Radar Imagery XXIV, 2017.

6. I. Bayram, E. Mason and B. Yazici, "A weakly-convex formulation for phaseless imaging," 2017 IEEE International Conference on Acoustics, Speech and Signal Processing (ICASSP), New Orleans, LA, 2017, pp. 6045-6049.

7. E. Mason and B. Yazici, Robustness of LRMR based Passive Radar Imaging to Phase Errors," Proceedings of EUSAR 2016: 11th European Conference on Synthetic Aperture Radar, Hamburg, Germany, pp. 1-4, 2016.

8. E. Mason, B. Yazici, "Moving Target Imaging using Sparse and Low- Rank Structure," Proceedings of SPIE Defense and Security Conference, Baltimore, MD, April 2016.

- In August 2016, I attended NSF Industry/University Center for Research Collaboration (I/UCRC) on ATR in Wright State University, Dayton OH. I talked to Ed Zelnio of AFRL, Profs. Lee Potter of Ohio State University and Al Hero of University of Michigan about our research project to support my student Eric Mason. Our research project was rated very highly by industry participants and funded for a year.

- In February 2017, I was invited to attend ONR's Ocean Engineering and Marine Systems Program Review in St. Augustine, FL. The projects presented ranged from synthetic aperture sonar (SAS) image reconstruction to machine learning using SAS imagery. I met researchers from Naval Warefare Center (Dr. James Prater), Panama City, FL and University of Washington, Applied Physics laboratory (Dr. Tim Marston), Seattle, WA working on SAS image reconstruction. We discussed circular synthetic aperture image reconstruction and other SAR related issues. I pointed out many of my publications to NWC and APL researchers. I also chatted with faculty from Georgia Tech, Pennsylvania State University and industry on machine learning. I pointed out the body of work on ATR in radar and encouraged SAS community to contact AFRL on ATR.

- In May 2017, I attended IEEE Radar Conference in Seattle, WA. Every year, I serve in the technical committee of IEEE Radar Conference. This year I managed review of radar signal processing papers. The conference was very well organized, well attended and included high quality papers

not only from US researchers, but also from international participants. I presented three papers and chaired three sessions, two on SAR and one on machine learning. There was a great deal of interest in our paper entitled "Deep Learning for Radar". I observed, in general, that there is a growing interest in machine learning techniques in radar. As always I renewed my acquaintance with AFRL researchers, colleagues from academia and researchers from industry and other national labs. Dr. Heiner Kuschel of DLR invited me to take part in NATO SET panel on passive radar. I completed all paper work, but I found out that the panel is classified and it would not be possible for me to attend without clearance. I was reached out by another NATO SET panel lead by Prof. Marco Mortarello of Pisa University on Compressive Sensing for Radar. I was also invited to give talks at Penn State Unv. and AFRL on my research.

- In June 2017, I attended IEEE International Radar Symposium (IRS) in Prague, Czech Republic per Dr. Kryzstof Kulpa's (of Warsaw University of Technology) invitation. This is a meeting attended primarily by European researchers. I presented our work on polarimetric radar which was very attentively listened. Prof. Kulpa invited me to visit Warsaw University of Technology to give talks. He also expressed interest in sending some of his PhD students to visit my research group. I also met my former post-doc Dr. Ling Wang and Prof. Jochaim Ender (a mathematician working on radar) in the symposium.

- My then student Eric Mason attended IEEE International Conference on Acoustics and Signal Processing (ICASSP) in March 2017 and presented our paper on weakly convex optimization on phaseless imaging. Eric also attended SPIE Defense and Security Conference in Anaheim, CA and presented our work deep learning in Ed Zelnio's SAR symposium. Additionally, Eric spent the summer of 2016 as an intern at AFRL ATR Center. He attended the IUCRC meetings in August 2016 and February 2017 and presented progress in his research.

3.2 Activities in 2017-2018

I had limited travel this year due to health issues, but my students attended the IEEE Radar Conference in Oklahoma City, OK and SPIE Defense and Security

Conference in Anaheim, CA. In these meetings, the following papers were presented:

1. B. Yonel, E. Mason, B. Yazıcı, "Passive Phaseless SAR Imaging," 2018 Asilomar Conference, Pacific Grove, CA, 2018.

2. B. Yonel, I.Y. Son, B Yazıcı, "Generalized Wirtinger flow for passive polarimetric reconstruction of extended dipole targets," IEEE Radar Conference (RadarConf18), pp: 1353 - 1358, 2018.

3. B. Yonel, E. Mason, B. Yazıcı, "Deep learning for waveform estimation in passive synthetic aperture radar imaging, " Algorithms for Synthetic Aperture Radar Imagery XXV 10647, 106470E, 2018.

4. B. Yonel, E. Mason, B. Yazıcı, "Deep learning for waveform estimation in passive synthetic aperture radar," IEEE Radar Conference (RadarConf18), pp: 1395 - 1400, 2018.

5. E. Mason, B. Yazıcı, "Passive Phaseless SAR Imaging," 2018 IEEE Radar Conference (RadarConf18), pp: 0292 - 0297, 2018.

- In September 2017, I visited Penn State University and gave a talk on Deep Learning for computational imaging per my colleague Prof. Vishal Monga's invitation. Vishal's students gave me presentations describing their projects in detail. Vishal and I both thought of combining our expertise and collaborating on projects involving imaging and automatic target recognition.

- In October 2017, I was re-elected to serve in IEEE Signal Processing Society Technical Committee on Signal Processing Methods and Theory for the next three years. Additionally, I was elected and start serving in the following IEEE Signal Processing Society Technical Committees:

  - Technical Committee on Sensor Array Multichannel, 2018-2020.
  - Special Interest Group on Computational Imaging, 2018-2021.

- In January 2018, I was elected to serve as an associate editor to IEEE Transactions in Computational Imaging for the next four years.

- As in 2017, in February 2018, I was invited to attend ONR's Ocean Engineering and Marine Systems Program Review in St. Augustine, FL. This time I attended the meeting as a PI sponsored by the Ocean Engineering and Marine Systems Program. I renewed my acquaintances with Dr. Prater of Naval Surface Warfare Center and Dr. Marston of University of Washington, Applied Physics laboratory. I met a group of your researchers from NSWC, Panama City, one of whom, Dr. Denton Woods, later helped me to access a high fidelity synthetic aperture sonar data simulator. I also chatted with my colleague and friend Vishal Monga who is also sponsored by the same ONR program. We discussed several ideas and topics of collaboration.

- In March 2018, my student Bariscan and I took part in a workshop (organized by Prof. Ge Wang) on Deep Learning held at RPI. Our work drew interest from attendees and we were invited to give a talk to the medical imaging program in General Electric Research Center, Niskayuna, NY.

- In April 2018, my former PhD student, Eric Mason and current students, Bariscan Yonel and Il-Young Son attended IEEE Radar Conference in Oklahoma City, OK. As always, I served in the Technical Committee of the IEEE Radar Conference. Eric presented a paper entitled "Phaseless Passive SAR Imaging" which apparently drew significant interest from the attendees. Eric and Bariscan presented "Deep learning for waveform estimation in passive synthetic aperture radar," and Bariscan and Il-Young presented "Generalized Wirtinger flow for passive polarimetric reconstruction of extended dipole targets". We are currently drafting journal papers on all three topics. Eric also presented our Deep Learning based waveform estimation work in Ed Zelnio's SAR symposium in SPIE Defense and Security Conference in Anaheim, CA.

- In April 2018, Dr. Mike Wicks visited me at RPI. He gave a talk on his research. As always Mike had many different ideas and we discussed collaboration opportunities.

3.3 Activities in 2018-2019

My students and I attended the IEEE Radar Conference in Boston, MA and IEEE International Radar Symposium, Aachen, Germany. In these meetings, the following papers were presented:

1. B. Yonel, I.Y. Son, B. Yazıcı, "Multistatic passive imaging via Wirtinger Flow," **Invited** IEEE International Radar Symposium, Aachen, Germany, 2019.

2. B. Yonel, S. Kazemi, B. Yazıcı, "A Neural Network Based Approach for Radar Imaging Beyond Born Approximation," 2019 IEEE Radar Conference, Boston, MA, 2019.

3. S. Kazemi, B. Yonel, B. Yazıcı, "Deep Learning for Direct Automatic Target Recognition from SAR Data," **Invited**. 2019 IEEE Radar Conference, Boston, MA, 2019.

- In January 2019, I was invited to attend ONR's Ocean Engineering and Marine Systems Program Review in St. Augustine, FL. I presented our recent results on segmentation and classification of objects using synthetic aperture sonar received data bypassing the image reconstruction step using machine learning methods. Our results were well received by the audience and the researchers at NSWC, San Diego CA and NSWC, Panama City, FL. I met the new program managers Dr. Daniel Cook and Dr. Tory Cobb and chatted with them about our on-going work.

- From February 2019 through May 2019, I was on sabbatical at The Center for Sensor Systems, University of Siegen, Siegen, Germany. The center is lead by Prof. Otmar Loffeld and has 21 faculty members who pursue research in a wide range of applications involving variety of electromagnetic sensors. Some of these projects are on developing novel sensors and others are on developing new and novel measurement and processing methods. I was invited and hosted by Prof. Otmar Loffeld. Prof. Loffeld's research group pursues both experimental and signal processing projects on radar remote sensing. Some of his projects include the design and implementation of passive bi-static radar using TerraSAR-X as an illumination of opportunity, multi-channel SAR sensor with applications to SAR interferometry and compressive sensing methods for SAR. I presented a number of seminars on my research during my stay at Siegen some of which included microlocal analysis in SAR imaging and its implications in design of novel SAR interferometric methods, non-convex provably exact methods in interferometric inversion and phaseless SAR imaging. My research

project most closely resonated with the research of the guest faculty member, Dr. Jochaim Ender. Dr. Ender is a mathematician who works/consults for German Space Agency and Fraunhoffer Research Institute. He visits Unv. of Siegen once a week to pursue academic research. At the time of my visit, Dr. Ender's research interest was on Inverse Synthetic Aperture Radar (ISAR). The main problem in ISAR is the estimation of the target's rational angles and shift in three-dimensional space which inherently introduces unknown phase angles. This problem at first appeared as a perfect application for phaseless imaging. Upon working on the problem formulation, I discovered an interesting generalization of the phaseless imaging problem and a novel solution for ISAR imaging with unknown rotation and shift. The key ideas involve modeling ISAR forward model on the Euclidean motion group and considering only the "magnitude" of the Fourier transform of the measurements over the Euclidean group. This is identical to the phaseless imaging problem in which one considers only the magnitude data with respect to the ordinary Fourier transform (i.e., the Fourier transform of the additive group over the real numbers). Here, the concept of "magnitude" is simply the composition of the matrix valued Euclidean group Fourier "coefficients" and their adjoint matrix. I was pleasantly surprised by such a generalization of the phaseless imaging problem and its relevance to an important imaging application. I drafted a note on this idea and hope to find a mathematically oriented student to implement the method.

- My student presented our work on interferometric inversion in the IEEE Radar Symposium in Aachen Germany.

- In April 2019, I organized an invited session on machine learning and radar sensing and imaging in the 2019 IEEE Radar Conference, Boston, MA. The invited papers ranged from ATR to image reconstruction. There was a very strong interest in the session across the entire radar signal processing community.

Chapter 4

Specific Technical Findings

4.1 List of Publications in the Period 2016-2019

The research presented in the following publications are funded by the AFOSR grant.

Book Chapters

B1. E. Mason, I. Bayram, B. Yazici, "Optimization Methods for Synthetic Aperture Radar Imaging," to be published in Handbook of Convex Optimization Methods in Imaging Science by Springer-Verlag in 2018.

B2. S. Kazemi, E. Mason, B. Yonel, B. Yazıcı, "Deep Learning for Passive Synthetic Aperture Radar Imaging," to appear in IET book on Deep Neural Networks for Radar Applications, pp. 1-27, 2020.

Journal Publications

J1. B. Yonel and B. Yazıcı, " A Deterministic Convergence Framework for Exact Non-Convex Phase Retrieval," to appear in the *IEEE Transactions on Signal Processing*, December 2019.

J2. B. Yonel, I.Y. Son, B. Yazıcı, "Exact Multistatic Interferometric Inversion via Generalized Wirtinger Flow," *IEEE Transactions on Computational Imaging*, vol. 6, pp. 711-726, 2020.

J3. B. Yonel, B. Yazıcı, "Generalized Wirtinger Flow for Interferometric Inversion," *SIAM Imaging Science Journal*, 2019 12 (4), 2119-2164, 2019.

J4. L. Wang and B. Yazıcı, "Analysis of Artifacts in SAR Imagery due to Fluctuation in Refractive Index," *IEEE Trans on Computational Imaging,* Vol. 5 , Issue: 3 , pp: 450 - 464, Sept. 2019

J5. B. Yonel, E. Mason, B. Yazıcı, "Deep Learning for Waveform Estimation and Imaging in Passive Radar," *IET Radar, Sonar and Navigation Journal*, [**invited**] Special issue on Passive High Resolution Radar Imaging, 13.6 (2019): 915-926, February 2019.

J6. S. Wacks, B. Yazıcı, "Doppler-DPCA and Doppler-ATI: Novel SAR Modalities for Imaging of Moving Targets Using Ultra-Narrowband Waveforms" *IEEE Transactions on Computational Imaging*, Vol. 4, Issue 1, pp. 125-136, March 2018.

J7. B. Yazıcı, I.Y. Son, H.C. Yanik "Doppler Synthetic Aperture Interferometry: A Novel Synthetic Aperture Interferometry for Height Mapping using Ultra-Narrowband Continuous Waveforms" *Inverse Problems Journal*, 34 (2018) 055003 (28pp), March 2018.

J8. B. Yonel, E. Mason, B. Yazıcı, "Deep Learning for Passive Synthetic Aperture Radar," [**invited**] *IEEE Trans. on Selected Topics in SP - Machine Learning for RF Communication and Radar*, Vol. 12, No. 1, pp. 90-103, February 2018.

J9. L. Wang, B. Yazıcı, "Layover Analysis in Synthetic Aperture Imagery," *SIAM Imaging Science Journal*, 10(3), 1033 - 1068. (36 pages), 2017.

J10. I.Y. Son, and B. Yazıcı, "Passive polarimetric multistatic radar detection of moving targets." *Available Online*, arXiv preprint arXiv:1706.09369.

Conference Publications

C1. S. Kazemi, B. Yazıcı, "Deep Learning for joint SAR Image Reconstruction and Segmentation," in the Proceedings of IEEE International Radar Conference, 2020.

C2. B. Yonel, I.Y. Son, B. Yazıcı, "Multistatic passive imaging via Wirtinger Flow," **Invited** IEEE International Radar Symposium, Aachen, Germany, 2019.

C3. B. Yonel, S. Kazemi, B. Yazıcı, "A Neural Network Based Approach for Radar Imaging Beyond Born Approximation," 2019 IEEE Radar Conference, Boston, MA, 2019.

C4. S. Kazemi, B. Yonel, B. Yazıcı, "Deep Learning for Direct Automatic Target Recognition from SAR Data," **Invited**. 2019 IEEE Radar Conference, Boston, MA, 2019.

C5. B. Yonel, E. Mason, B. Yazıcı, "Phaseless Passive Synthetic Aperture Radar Imaging via Wirtinger Flow," **Invited**. 2018 Asilomar Conference, Pacific Grove, CA, 2018.

C6. B. Yonel, E. Mason, B Yazıcı, "Passive SAR Imaging using Phaseless Measurements," Proceedings of European Conference on Synthetic Aperture Radar, Aachen, Germany, 2018.

C7. B. Yonel, E. Mason, B Yazıcı, "Generalized Wirtinger flow for passive polarimetric reconstruction of extended dipole targets," IEEE Radar Conference (RadarConf18), pp: 1353 - 1358, 2018.

C8. B. Yonel, E. Mason, B. Yazıcı, "Deep learning for waveform estimation in passive synthetic aperture radar imaging, " Algorithms for Synthetic Aperture Radar Imagery XXV 10647, 106470E, 2018.

C9. B. Yonel, E. Mason, B. Yazıcı, "Deep learning for waveform estimation in passive synthetic aperture radar," IEEE Radar Conference (RadarConf18), pp: 1395 - 1400, 2018.

C10. E. Mason, B. Yazıcı, "Passive Phaseless SAR Imaging," 2018 IEEE Radar Conference (RadarConf18), pp: 0292 - 0297, 2018.

C11. L. Wang, and B. Yazıcı, "Height reconstruction using differential layover for SAR imagery," IEEE Radar Conference pp. 0169-0174, 2017.

C12. L. Wang, and B. Yazıcı, "Effects of fluctuation in refractive index of atmosphere on synthetic aperture radar images," IEEE Radar Conference pp. 0163-0168, 2017.

C13. I.Y. Son, and B. Yazıcı, "Passive Polarimetric Reconstruction of Extended Dipole Target," International Radar Symposium, pp. 1-10, June 2017.

C14. E. Mason, B. Yonel, and B. Yazıcı, "Deep learning for radar," in the Proceedings of 2017 IEEE Radar Conference, May 2017, pp. 17031708.

C15. E. Mason, B. Yonel, and B. Yazıcı, "Deep learning for SAR image formation," in Proc.SPIE, vol. 10201, 2017.

C16. I. Bayram, E. Mason, and B. B. Yazıcı, "A weakly-convex formulation for phaseless imaging," in IEEE International Conference on Acoustics, Speech and Signal Processing (ICASSP), March 2017, pp. 6045 - 6049.

C17. E. Mason, B. Yazıcı "Robustness of LRMR based Passive Radar Imaging to Phase Errors," Proceedings of EUSAR 2016: 11th European Conference on Synthetic Aperture Radar, Hamburg, Germany, 2016.

C18. Il-Young Son, B. Yazıcı "Passive Polarimetric Multi-static Radar for Ground Moving Target" in the Proceedings of *IEEE Radar*, 2016.

C19. E. Mason, B. Yazıcı "Moving Target Imaging using Sparse and Low-rank Structures" in the Proceedings of *SPIE Defense and Security*, 2016.

4.2 Description

From August 2016 until October 2019, we worked on the following specific problems:

- Analysis of SAR artifacts
- Doppler SAR interferometric imaging
- Multi-static and polarimetric passive radar imaging
- Phaseless imaging with applications to radar
- Convex and non-convex optimization methods for passive imaging
- Machine learning for inverse problems in imaging with applications in passive SAR and ATR

These topics are directly related to the objectives of the project outlined in the introduction.

4.2.1 Analysis of SAR Artifacts

Publications

J4. L. Wang and B. Yazıcı, "Analysis of Artifacts in SAR Imagery due to Fluctuation in Refractive Index," *IEEE Trans on Computational Imaging,* Vol. 5 , Issue: 3 , pp: 450 - 464, Sept. 2019

J9. L. Wang, B. Yazıcı, "Layover Analysis in Synthetic Aperture Imagery," *SIAM Imaging Science Journal*, 10(3), 1033 - 1068. (36 pages), 2017.

C11. L. Wang, and B. Yazıcı, "Height reconstruction using differential layover for SAR imagery," IEEE Radar Conference pp. 0169-0174, 2017.

C12. L. Wang, and B. Yazıcı, "Effects of fluctuation in refractive index of atmosphere on synthetic aperture radar images," IEEE Radar Conference pp. 0163-0168, 2017.

- **Analysis of Artifacts in SAR Imagery Due to Fluctuation in Refractive Index [J4], [C12]**: We analyze the artifacts in synthetic aperture radar imagery due to fluctuations in the refractive index of the atmosphere, specifically due to absorption and variations in speed of light. SAR image reconstruction algorithms ignore absorption and assume unit refractive index. We assume a complex-valued refractive index for the atmosphere and analyze the errors in reconstructed images due to absorption and fluctuations in the speed of electromagnetic (EM) waves. Absorption leads to amplitude errors, which can be viewed as a filtering error. This error can be characterized as systematic variations in the ground reflectivity function. Fluctuations in the speed of EM waves lead to phase errors, which manifest as positioning errors or geometric distortions in synthetic aperture radar (SAR) imagery.

- **Layover Analysis in Synthetic Aperture Imagery [J9], [C11]**: Layover is an artifact observed in synthetic aperture radar (SAR) images. This artifact manifests as geometric distortions or positioning errors due to unknown or inaccurate ground topography information. Layover artifact results in erroneous distance between reconstructed scatterers, particularly in elevated regions. We develop a quantitative analysis of positioning errors due to incorrect height information in backprojection based (BP) SAR image formation. Our analysis is based on microlocal techniques and provides an explicit algebraic relationship between the two-dimensional positioning error

and height error. Our analysis is applicable to arbitrary imaging geometries including bistatic configuration, arbitrary antenna trajectories, wide apertures, and large scenes. While we focus primarily on BP based image formation, the results are also applicable to range-Doppler type image formation methods. Our results can be used to interpret and identify layover regions in SAR images and extract valuable information from layover artifacts. In [C11], we presented a method of utilizing layover artifacts for height estimation.

4.2.2 Doppler SAR Interferometry

Publications

J6. S. Wacks, B. Yazıcı, "Doppler-DPCA and Doppler-ATI: Novel SAR Modalities for Imaging of Moving Targets Using Ultra-Narrowband Waveforms" *IEEE Transactions on Computational Imaging*, Vol. 4, Issue 1, pp. 125-136, March 2018.

J7. B. Yazıcı, I.Y. Son, H.C. Yanik "Doppler Synthetic Aperture Interferometry: A Novel Synthetic Aperture Interferometry for Height Mapping using Ultra-Narrowband Continuous Waveforms" *Inverse Problems Journal*, 34 (2018) 055003 (28pp), March 2018.

- **Doppler synthetic aperture radar interferometry: A novel SAR interferometry for height mapping using ultra-narrowband waveforms [J7]**: We introduced a new and novel radar interferometry based on Doppler synthetic aperture radar (Doppler-SAR) paradigm. Conventional SAR interferometry relies on wideband transmitted waveforms to obtain high range resolution. Topography of a surface is directly related to the range difference between two antennas configured at different positions. Doppler-SAR is a novel imaging modality that uses ultra-narrowband continuous waves (UNCW). It takes advantage of high resolution Doppler information provided by UNCWs to form high resolution SAR images. We introduce the theory of Doppler-SAR interferometry. We derive an interferometric phase model and develop the equations of height mapping. Unlike conventional SAR interferometry, we show that the topography of a scene is related to the difference in Doppler frequency between two antennas configured at different velocities. While the conventional SAR interferometry uses range, Doppler and Doppler due to interferometric phase in height mapping;

Doppler-SAR interferometry uses Doppler, Doppler-rate and Doppler-rate due to interferometric phase in height mapping. Doppler-SAR interferometry offers the advantages of long-range, robust, environmentally friendly operations; low-power, low-cost, lightweight systems suitable for low-payload platforms, such as micro-satellites; and passive applications using sources of opportunity transmitting UNCW.

- **Doppler-DPCA and Doppler-ATI: Novel SAR Modalities for Imaging of Moving Targets Using Ultra-Narrowband Waveforms [J6]**: We introduced two novel imaging modalities: Doppler displaced phase center antenna (Doppler-DPCA) and Doppler along track interferometry (Doppler-ATI). The DPCA and ATI techniques have the distinct advantage of removing the response from stationary targets (clutter). We develop DPCA and ATI techniques in Doppler synthetic aperture radar (Doppler-SAR) paradigm to image moving targets embedded in clutter. Doppler-SAR uses ultra-narrowband continuous waveforms (UNCW) to reconstruct high-resolution SAR images. We consider a two-channel bistatic configuration with a stationary antenna transmitting UNCW and two receiving antennas moving along an arbitrary trajectory in tandem. We introduced the theory for Doppler-DPCA and Doppler-ATI. We derive an interferometric phase model and develop equations of velocity mapping. While conventional wideband SAR DPCA and ATI use range difference, Doppler-DPCA and Doppler-ATI use high-resolution temporal Doppler difference in imaging of moving targets. These novel modalities can be used for applications requiring high signal-to-noise ratio, long-range, low-power, and low payload such as microsatellites and uninhabited aerial vehicles; passive imaging using sources of opportunity, such as TV and radio stations; and in applications requiring spectrum efficiency.

4.2.3 Multi-static and Polarimetric Radar Imaging

Publications

J2. B. Yonel, I.Y. Son, B. Yazıcı, "Exact Multistatic Interferometric Inversion via Generalized Wirtinger Flow," *IEEE Transactions on Computational Imaging*, vol. 6, pp. 711-726, 2020.

J10. I.Y. Son, and B. Yazıcı, "Passive polarimetric multistatic radar detection of moving targets." *Available Online*, arXiv preprint arXiv:1706.09369.

C2. B. Yonel, I.Y. Son, B. Yazıcı, "Multistatic passive imaging via Wirtinger Flow," **Invited** IEEE International Radar Symposium, Aachen, Germany, 2019.

C7. B. Yonel, E. Mason, B Yazıcı, "Generalized Wirtinger flow for passive polarimetric reconstruction of extended dipole targets," IEEE Radar Conference (RadarConf18), pp: 1353 - 1358, 2018.

C13. I.Y. Son, and B. Yazıcı, "Passive Polarimetric Reconstruction of Extended Dipole Target," International Radar Symposium, pp. 1-10, June 2017.

C18. I.Y. Son, B. Yazıcı "Passive Polarimetric Multi-static Radar for Ground Moving Target" in the Proceedings of *IEEE Radar*, 2016.

- **Exact Multistatic Interferometric Imaging via Generalized Wirtinger Flow [J2], [C2], [C7]**: We present a novel, exact method to address the interferometric inversion problem for multistatic wave-based imaging based on Generalized Wirtinger Flow (GWF). Interferometric imaging is a relative of phase retrieval, which arises from cross-correlating measurements from pairs of receivers. GWF provides a theoretical framework to process scattering data satisfying the Born approximation, and guarantees exact recovery of the underlying scene reflectivity vector from interferometric measurements if the discretized lifted forward model satisfies the restricted isometry property over rank-1, positive semi-definite matrices with a sufficiently small restricted isometry constant (RIC). To this end, we design a linear deterministic discrete lifted forward model for interferometric multistatic radar measurements such that the exact recovery conditions of GWF are satisfied. Our results identify a lower limit on the pixel spacing and the sample complexity for exact multistatic radar imaging. We provide a numerical study of our RIC and pixel spacing bounds on synthetic single scattering data, which show that GWF can achieve exact recovery with super-resolution. While our primary interest lies in radar imaging, our results are applicable to other multistatic wave-based imaging problems such as those arising in acoustics and geophysics.

- **Passive Polarimetric Multistatic Radar Detection of Moving Targets [J10], [C13], [C18]**: We study the exploitation of polarimetric diversity in passive multistatic radar for detecting moving targets. We first derive a data model that takes into account polarization and anisotropy of targets inherent in multistatic configurations. Unlike conventional isotropic models

in which targets are modeled as a collection of uniform spheres, we model targets as a collection of dipole antennas with unknown directions. We consider a multistatic configuration in which each receiver is equipped with a pair of orthogonally polarized antennas, one directed to a scene of interest collecting target-path signal and another one having a direct line-of-sight to a transmitter-of-opportunity collecting direct-path signal. We formulate the detection of moving target problem in a generalized likelihood ratio test framework under the assumption that direct-path signal is available. We show that the result can be reduced to the case in which the direct-path signal is absent. We present a method for estimating the dipole moments of targets. Extensive numerical simulations show the performance of both the detection and the dipole estimation tasks with and without polarimetric diversity.

4.2.4 Convex and Non-Convex Methods for Passive Imaging

Publications

B1. E. Mason, I. Bayram, B. Yazici, "Optimization Methods for Synthetic Aperture Radar Imaging," to be published in Handbook of Convex Optimization Methods in Imaging Science by Springer-Verlag in 2018.

J2. B. Yonel, I.Y. Son, B. Yazıcı, "Exact Multistatic Interferometric Inversion via Generalized Wirtinger Flow," *IEEE Transactions on Computational Imaging*, vol. 6, pp. 711-726, 2020.

J3. B. Yonel, B. Yazıcı, "Generalized Wirtinger Flow for Interferometric Inversion," *SIAM Imaging Science Journal*, 2019 12 (4), 2119-2164, 2019.

C2. B. Yonel, I.Y. Son, B. Yazıcı, "Multistatic passive imaging via Wirtinger Flow," **Invited** IEEE International Radar Symposium, Aachen, Germany, 2019.

C7. B. Yonel, E. Mason, B Yazıcı, "Generalized Wirtinger flow for passive polarimetric reconstruction of extended dipole targets," IEEE Radar Conference (RadarConf18), pp: 1353 - 1358, 2018.

C16. I. Bayram, E. Mason, and B. B. Yazıcı, "A weakly-convex formulation for phaseless imaging," in IEEE International Conference on Acoustics, Speech and Signal Processing (ICASSP), March 2017, pp. 6045 - 6049.

C17. E. Mason, B. Yazıcı "Robustness of LRMR based Passive Radar Imaging to Phase Errors," Proceedings of EUSAR 2016: 11th European Conference on Synthetic Aperture Radar, Hamburg, Germany, 2016.

C19. E. Mason, B. Yazıcı "Moving Target Imaging using Sparse and Low-rank Structures" in the Proceedings of *SPIE Defense and Security*, 2016.

- **Passive SAR Imaging Using Low-rank Matrix Recovery Methods [B1], [C17], [C19]:** We present a novel image formation method for passive synthetic aperture radar (SAR) imaging for both moving and stationary targets. The method is an alternative to widely used time difference of arrival (TDOA) or correlation-based backprojection method. These methods work under the assumption that the scene is composed of a single or a few widely separated point targets. The new method overcomes this limitation and can reconstruct heterogeneous scenes with extended targets. We assume that the scene of interest is illuminated by a stationary transmitter of opportunity with known illumination direction, but unknown location. We consider two airborne receivers and correlate the fast-time bistatic measurements at each slow-time. This correlation process maps the tensor product of the scene reflectivity with itself to the correlated measurements. Since this tensor product is a rank-one positive semi-definite operator, the image formation lends itself to low-rank matrix recovery techniques. Taking into account additive noise in bistatic measurements, we formulate the estimation of the rank-one operator as a convex optimization with rank constrain. We present a gradient-descent based iterative reconstruction algorithm and analyze its computational complexity. Extensive numerical simulations show that the new method is superior to correlation-based backprojection in reconstructing extended and distributed targets with better geometric fidelity, sharper edges, and better noise suppression.

- **Generalized Wintinger Flow for interferometric inversion with applications in passive radar imaging [J3]:**

  Generalized phase retrieval is a ubiquitous problem in many disciplines. The problem consists of recovery of a signal from *auto*-correlations of its linear transformations. In [J3], my student Bariscan and I investigate a problem that is a close relative of phase retrieval: interferometric inversion, i.e., recovery of a signal from *cross*-correlations of its linear transformations. In recent years, phase retrieval literature has undergone significant advancements through the introduction of provably good methods. A prominent

method of interest is the Wirtinger Flow [1], in which phase retrieval problem is solved in a provably exact manner by a non-convex optimization problem. We pursue this framework for interferometric inversion problem and develop Generalized Wirtinger Flow, and provide the exact recovery guarantees for a general complex signal. In achieving this, we take a low rank recovery perspective to interferometric inversion, in which the problem is *lifted* to a higher dimensional rank-1 subspace recovery. We identify key condition that the interferometric measurement mapping should satisfy in the lifted problem as the matrix restricted isometry property over rank-1 positive semi-definite matrices (RIP-1). We show that RIP-1 condition is a sufficient condition for exact recovery by GWF as long as the restricted isometry constant is within the upper bound of 0.256. We then establish the validity of the condition for cross correlations of linear measurements collected by complex Gaussian sampling vectors.

Finally, we establish the RIP-1 condition for cross correlations of linear measurements collected by complex Gaussian sampling vectors. We illustrate the validity of our analysis on complex Gaussian sampling vectors through numerical simulations, and display the effectiveness of our method on the passive synthetic aperture radar imaging problem, for which a RIP-1 has been previously established.

In [C7], under the observation that generalized phase retrieval is a special case of cross-correlation measurement model, my students Bariscan, Il-Young and I propose Wirtinger flow method for passive polarimetric imaging from interferometric measurements. We consider the polarimetric imaging problem for a distributed array of antennas, in which scene reflectivities and polarization states of stationary targets have to be simultaneously reconstructed. Linear measurements collected from each antenna is correlated with the others to yield a quadratic measurement model. We then pursue the non-convex approach rather than the previously explored LRMR method, and derive Generalized Wirtinger flow for cross-correlated measurements.

4.2.5 Phaseless Imaging with Applications to Passive Radar

Publications

[1] E.J. Candes, X. Li, M. Soltanolkotabi, "Phase retrieval via wirtinger flow: Theory and algorithms", IEEE Transactions on Information Theory, vol. 61, no. 4, pp. 1985-2007, 2015.

J1. B. Yonel and B. Yazıcı, " A Deterministic Convergence Framework for Exact Non-Convex Phase Retrieval," to appear in the *IEEE Transactions on Signal Processing*, December 2019.

C5. B. Yonel, E. Mason, B. Yazıcı, "Phaseless Passive Synthetic Aperture Radar Imaging via Wirtinger Flow," **Invited**. 2018 Asilomar Conference, Pacific Grove, CA, 2018.

C6. B. Yonel, E. Mason, B Yazıcı, "Passive SAR Imaging using Phaseless Measurements," Proceedings of European Conference on Synthetic Aperture Radar, Aachen, Germany, 2018.

C10. E. Mason, B. Yazıcı, "Passive Phaseless SAR Imaging," 2018 IEEE Radar Conference (RadarConf18), pp: 0292 - 0297, 2018.

- **A Deterministic Convergence Framework for Exact Non-Convex Phase Retrieval [J1]:** In this work, we analyze the non-convex framework of Wirtinger Flow (WF) for phase retrieval and identify a novel sufficient condition for universal exact recovery through the lens of low rank matrix recovery theory. Via a perspective in the lifted domain, we establish that the convergence of WF to a true solution is geometrically implied under a condition on the lifted forward model which relates to the concentration of the spectral matrix around its expectation given that the bound is sufficiently tight. As a result, a deterministic relationship between accuracy of spectral initialization and the validity of *the regularity condition* is derived, and a convergence rate that solely depends on the concentration bound is obtained. Notably, the developed framework addresses a theoretical gap in non-convex optimization literature on solving quadratic systems of equations with the convergence arguments that are deterministic. Finally, we quantify a lower bound on the signal-to-noise ratio such that theoretical guarantees are valid using the spectral initialization even in the absence of pre-processing or sample truncation.

- **Phaseless SAR imaging [C5], [C6], [C10]:** Passive synthetic aperture radar (SAR) is a coherent imaging method. Thus, performance is very susceptible to phase error, which result because the transmitter is not under control of the user. These errors result from poor clock synchronization, uncertainty in transmitter location and trajectory error, to name a few. In [C5],[C6] and [C10], we present an incoherent imaging method for passive

SAR which uses phaseless measurements. The approach is appealing over existing methods for passive radar since only a single receiver is required, and robustness to uncertainties is increased. We utilize the observation that the squared modulus of the data is equivalent to a linear mapping of a rank-one positive semi-definite operator, formed as the tensor product of scene reflectivity with itself. Therefore, we pose imaging as least-squares optimization, utilizing this structure to constrain the problem. We consider the use of both convex and non-convex constraints, for which we provide efficient and provably convergent iterative schemes.

This effort was initiated by Eric. Eric, Bariscan and I are currently working on a journal paper on this topic.

4.2.6 Machine Learning for Inverse Problems in Radar Imaging

Publications

B2. S. Kazemi, E. Mason, B. Yonel, B. Yazıcı, "Deep Learning for Passive Synthetic Aperture Radar Imaging," to appear in IET book on Deep Neural Networks for Radar Applications, pp. 1-27, 2020.

J5. B. Yonel, E. Mason, B. Yazıcı, "Deep Learning for Waveform Estimation and Imaging in Passive Radar," *IET Radar, Sonar and Navigation Journal*, [**invited**] Special issue on Passive High Resolution Radar Imaging, 13.6 (2019): 915-926, February 2019.

J8. B. Yonel, E. Mason, B. Yazıcı, "Deep Learning for Passive Synthetic Aperture Radar," [**invited**] *IEEE Trans. on Selected Topics in SP - Machine Learning for RF Communication and Radar*, Vol. 12, No. 1, pp. 90-103, February 2018.

C1. S. Kazemi, B. Yazıcı, "Deep Learning for joint SAR Image Reconstruction and Segmentation," in the Proceedings of IEEE International Radar Conference, 2020.

C3. B. Yonel, S. Kazemi, B. Yazıcı, "A Neural Network Based Approach for Radar Imaging Beyond Born Approximation," 2019 IEEE Radar Conference, Boston, MA, 2019.

C4. S. Kazemi, B. Yonel, B. Yazıcı, "Deep Learning for Direct Automatic Target Recognition from SAR Data," **Invited**. 2019 IEEE Radar Conference, Boston, MA, 2019.

C8. B. Yonel, E. Mason, B. Yazıcı, "Deep learning for waveform estimation in passive synthetic aperture radar imaging, " Algorithms for Synthetic Aperture Radar Imagery XXV 10647, 106470E, 2018.

C9. B. Yonel, E. Mason, B. Yazıcı, "Deep learning for waveform estimation in passive synthetic aperture radar," IEEE Radar Conference (RadarConf18), pp: 1395 - 1400, 2018.

C14. E. Mason, B. Yonel, and B. Yazıcı, "Deep learning for radar," in 2017 IEEE Radar Conference, May 2017, pp. 17031708.

C15. E. Mason, B. Yonel, and B. Yazıcı, "Deep learning for SAR image formation," in Proc.SPIE, vol. 10201, 2017.

- **Machine Learning for Passive SAR Imaging [B2], [J5], [J8], [C9], [C14], [C15]:** Deep learning (DL) has dramatically advanced the state-of-the-art in many challenging problems in different domains of science including in speech recognition, visual object recognition, predicting the activity of drug molecules, reconstructing brain circuits, and many other problems. Motivated by these advances, in [J8] we introduced a deep learning based mathematical framework for inverse problems in imaging, and demonstrate the advantages and applicability of our approach in passive SAR image reconstruction. Imaging problems require physics-based modeling of sensing and estimation via optimization. This separation between modeling and estimation is largely due to different domains of expertise. In this project we move away from the dichotomy between modeling and optimization and propose a novel learning framework in which modeling and optimization parameters are jointly learned and refined. Our approach is particularly suitable for a class of image formation problems in which the forward model is only partially known. We demonstrate through extensive numerical simulations that our DL based approach out performs conventional sparse coding methods in terms of computational requirements and reconstructed image quality.

  In [J8], we considered the passive imaging problem in which the transmitter location is unknown, and used DL to refine the phase component of the

synthetic aperture radar (SAR) forward model. In [J5] we develop a DL-based approach for passive SAR image reconstruction when the transmitted waveforms of opportunity are unknown. Specifically we present a deep network architecture and an unsupervised training scheme to learn transmitted waveforms as a parameter of the SAR imaging problem, while reconstructing focused imagery. The key advantage of our approach as compared to other methods is that it only requires a single receiver antenna, thereby providing reduced cost and increased versatility. We extended our preliminary studies on the joint waveform estimation and imaging problem in [B2], developed the theory and demonstrate its effectiveness in extensive numerical simulations.

- **Machine Learning for SAR ATR [C1], [C4]:** Based on the framework for deep learning (DL) based image reconstruction approach for synthetic aperture radar (SAR) that we introduced in [J5] and [J8], we developed a recurrent neural network (RNN) based approach for direct automatic target recognition (ATR) from SAR received signal [C4]. The deep nonlinear network structure enables the modelling of the complex non-linear mapping from the input SAR/SAS received signal to the classification label. In developing the DL approach for direct ATR, we combined a dictionary learning based classification approach using sparse representation with the model-based DL image reconstruction framework. The objective function of the underlying optimization problem contains a data fidelity term and a regularized term imposing the sparsity condition. The RNN network resulting from the unwrapping of fixed number of iterative gradient descent steps has the dictionary as its parameters implying that the training process provides its optimum value for estimates sparse vectors in fixed number of iteration steps with improving classification accuracy. The DL approach is verified on both simulated SAR data and PCSWAT simulated sonar data, and is shown to outperform contemporary methods at similar computational complexity level.

  In [C1], we developed a method for joint image reconstruction and segmentation where the segmentation step involves separating the surrounding background from the objects of interest. The goal of this segmentation is to assist in further processing steps such as ATR. The model-based approach requires formulating an optimization problem that jointly recovers the unknown scene reflectivity vector and a window that corresponds to the foreground part of the image. The regularization part of the objective function

is formulated by assuming a generalized Gaussian distribution for the unknown image given the window and a Gibbs distribution for the window vector. By setting the generalized Gaussian distribution parameters to appropriate values, we incorporate prior information, such as sparsity prior for the foreground and normal distribution prior for the background. By unfolding the step of an iterative gradient descent approach with alternating minimization steps, a corresponding RNN based deep network is derived where the regularized terms are incorporated via the nonlinear functions at each RNN stage. Numerical evaluation on simulated data is performed for establishing feasibility.

Chapter 5

Appendix A - Sub-Task lead by J. Christian

Subpixel Localization of Isolated Edges and Lines in Digital Images

Devin Renshaw[1] and John Christian[1]
[1]Mechanical, Aerospace, and Nuclear Engineering, Rensselaer Polytechnic Institute, Troy, NY 12180 USA

The localization of edges and lines in digital images is an important component in many image processing pipelines. Several approaches attempt to solve this problem at both the pixel level and subpixel level. While the subpixel methods are often necessary for applications requiring best-possible accuracy, they are often susceptible to noise, use iterative methods, or require pre-processing. This work investigates a unified framework for subpixel edge and line localization using Zernike moments with ramp-based and wedge-based signal models. The method described here is non-iterative and performs no pre-processing on the image. Moreover, this method is found to outperform the current state-of-the-art for digital images with common signal-to-noise ratios. Performance is demonstrated on both synthetic and real images.

***Index Terms*—edge localization, line localization, Zernike moments**

I. Introduction

DIGITAL images frequently contain valuable information about the real-world objects observed by a camera, telescope, or other optical system. This information may be used to understand, interpret, monitor, or analyze the properties of objects contained within the scene. Oftentimes, such analysis makes use of geometric image primitives—with edges and lines being especially common examples. Although pixel-level edge/line localization is often adequate, some applications demand higher accuracy and motivate the need for subpixel localization.

In this work, we treat both edges and lines as a local (and not global) concept, with each being identifiable by the 2D intensity pattern within a small image patch. An edge is defined as an image point whose neighborhood possesses an intensity discontinuity in one direction and not in the other. Likewise, a line is defined as in image point belonging to a bright (or dark) 1D path against a dark (or bright) background. The local concept of an edge/line used here is not to be confused with its global counterpart, which is the locus of edge/line points forming a 1D path within the image. Furthermore, because our definition of edge/line is local, the global path formed by the locus of edge/line points may be of arbitrary shape and need not be straight—although we do assume the edge/line is approximately straight within its local neighborhood.

The technique developed in this work is designed for the localization of isolated edges/lines. An *isolated* edge/line is defined here as an edge/line point haivng no other points belonging to another edge/line within its neighborhood.

Pixel-level edge localization is a ubiquitous image processing task, with a variety of techniques that can be found in almost every introductory text on image processing. Some popular methods are those of Sobel [1], Marr-Hildreth [2], and Canny [3]—although there are many more. Likewise, there are several methods available for subpixel edge localization. Many of these methods operate by refining a pixel-level edge guess into a subpixel-level estimate. The approaches for achieving such a subpixel correction vary, but generally belong to one of four different categories: moment-based [4], least-squares fitting [5], partial area effect [6], and interpolation [7].

This work presents a localization framework that is equally suitable to finding the subpixel location of edge and line points within a digital image. Our method belongs to the moment-based category of techniques. We refine recent work on improved edge localization with Zernike moments [8] and then extend this approach to the closely related problem of line localization. Unlike conventional subpixel edge localization methods using Zernike moments that assume an intensity step function [9], we model the underlying intensity function as a ramp (for an edge) or a wedge (for a line). The framework presented here is computationally efficient, non-iterative, and can be used within any imaging pipeline.

The remainder of this work is organized as follows. Section II introduces the coordinate frames and scaling conventions that are used in Section III to construct Zernike moments on local image patches. Section IV describes how to use these Zernike moments for the subpixel localization of both edges and lines. Performance of this approach is then demonstrated quantitatively on synthetic images (Section V) and qualitatively on real images (Section VI).

II. Coordinate Frames and Conventions

Suppose that we have a digital image with N rows and M columns, with pixel intensity values stored in a $N \times M$ array (for a monochrome image). Define the u–v coordinate system with the origin in the upper lefthand corner such that pixel centers occur at integer values of u and v. The u-direction is to the right (corresponding to column number) and the v-direction is down (corresponding to the row number). We presume in this work that a different algorithm (e.g., Sobel [1], Canny[3]) has already produced pixel-level estimates for either an edge or line location. Assuming such an algorithm has detected m such pixel locations, we denote the set of pixel-level guesses as $\{\tilde{u}_i, \tilde{v}_i\}_i^m \subset \mathbb{Z}^{*2}$ (where $\mathbb{Z}^*$ is the set of non-negative integers).

The algorithms presented in this work use a small image patch (e.g., 5×5 or 7×7) centered about a pixel-level estimate of an edge or line location to compute a small correction to that feature's location. The result is subpixel-level localization of a

point belonging to an edge or line. Furthermore, the moment-based methods to be discussed in Section III require the signal to be contained within the unit circle. Thus, data within each small image patch must be scaled to lie within the unit circle. For the i-th patch,

$$\bar{u} = \frac{2}{N_p}(u - \tilde{u}_i) \qquad \bar{v} = \frac{2}{N_p}(v - \tilde{v}_i), \tag{1}$$

where N_p is the size of the image patch (e.g., $N_p = 5$ is a 5×5 patch). We generally constrain N_p to be an odd integer, such that the pixel-level guess occurs at the center of the patch. This scaling ensures that $\|\bar{u}\| \leq 1$ and $\|\bar{v}\| \leq 1$ for every point within the square patch, and that $\bar{u}^2 + \bar{v}^2 \leq 1$ within the inscribed circle.

We also find it convenient to define a rotated version of the $\bar{u}$–$\bar{v}$ coordinate frame with an orientation dictated by the local normal of the edge or line. Define a frame with coordinate axes $\bar{u}'$ and $\bar{v}'$ that are rotated by an angle ψ relative to the unprimed frame (Fig. 1) such that the $\bar{u}'$ direction is parallel with the local edge/line normal and $\bar{v}'$ is parallel to the edge/line tangent. The direction $\bar{u}'$ is chosen to be positive in the direction from dark to bright for an edge. Alternatively, for lines, the positive $\bar{u}'$ direction is chosen to be from the patch center towards the line's center. Thus, by construction, the correction from the pixel-level guess to the subpixel line location is a small positive update along the $\bar{u}'$ direction. The subpixel update along the $\bar{u}'$ direction may be either positive or negative for an edge.

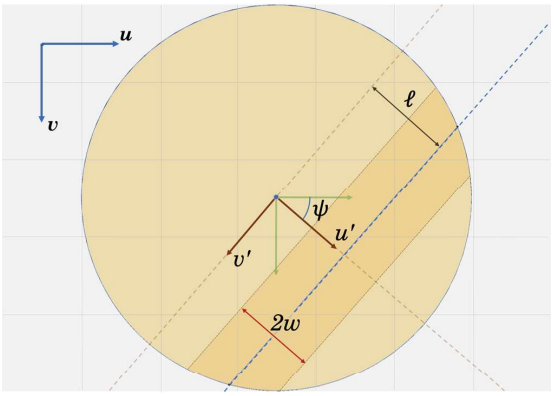

Fig. 1. Unaligned system in the uv frame, and the aligned prime frame $\bar{u}'\bar{v}'$, where $\bar{v}'$ is parallel to the incident line, and $\bar{u}'$ is normal to the line. Although this figure shows only an edge, these coordinate frame conventions are the same for both lines and edges.

III. Computation of Zernike Moments in Digital Images

It is well-established that image moments are a useful tool for compactly describing the shape of the 2D intensity pattern within an image patch using only a small number of parameters. In general, 2D moments are a weighted average of the 2D signal value, with the weights for a particular moment coming from its corresponding basis function. That is, given a basis function $P_{nm}(u, v)$, the corresponding moment of the arbitrary 2D signal $f(u, v)$ is computed as

$$\iint P_{nm}(\bar{u}, \bar{v}) f(\bar{u}, \bar{v})\, d\bar{u}\, d\bar{v} \tag{2}$$

Since we will be computing moments within small image patches, we have chosen to express all functions in terms of the scaled pixel coordinates $\{\bar{u}, \bar{v}\}$ as defined in Eq. 1.

The choice of basis functions P_{nm} is somewhat arbitrary, although it is desirable that the chosen set is both complete and orthogonal. In the case of edge or line localization, we are looking for basis function sets defined within the unit disk. If P_{nm} is chosen to be a polynomial in two variables, there are an infinite number of complete orthogonal sets [10]—with the Zernike polynomials being the most commonly used.

A. Zernike Polynomials

Zernike polynomials, originally developed to aid in the study of spherical aberrations in optical lenses [11], have since found uses for a broad array of applications [8], [12], [9], [13], [14], [15]. The Zernike polynomials may be written in either Cartesian or polar coordinates, with the polar form being the most commonly used,

$$P_{nm}(\rho, \theta) = R_{nm}(\rho)\ \exp(jm\theta) \tag{3}$$

where $j = \sqrt{-1}$ and

$$\rho^2 = \bar{u}^2 + \bar{v}^2 \tag{4}$$

$$R_{nm}(\rho) = \frac{\rho^{n-2s}}{(\frac{n-|m|}{2})!\rho^{|m|}} \frac{(n-s)!}{s!(\frac{n+|m|}{2}-1)!(\frac{n-|m|}{2}-s)!} \tag{5}$$

These polynomials form a complete set over a continuous space contained within the unit circle. The 1D radial polynomials, $R_{nm}(\rho)$, and their corresponding 2D Zernike polynomials, $P_{nm}(u, v)$, may be computed for a few common combinations of n and m,

$$R_{00}(\rho) = 1 \Rightarrow P_{00}(\bar{u}, \bar{v}) = 1, \tag{6}$$

$$R_{11}(\rho) = \rho \Rightarrow P_{11}(\bar{u}, \bar{v}) = \bar{u} + j\bar{v}, \tag{7}$$

$$R_{20}(\rho) = 2\rho^2 - 1 \Rightarrow P_{20}(\bar{u}, \bar{v}) = 2\bar{u}^2 + 2\bar{v}^2 - 1, \tag{8}$$

$$R_{22}(\rho) = \rho^2 \Rightarrow P_{22}(\bar{u}, \bar{v}) = \bar{u}^2 + \bar{v}^2. \tag{9}$$

where the order n and repetition m [8] (or angular dependence [16]) can assume any values that satisfy

$$n \geq |m| \geq 0, \tag{10}$$

$$n - m \quad even. \tag{11}$$

It is straightforward to show that Zernike polynomials are orthogonal under an L_2-inner product,

$$\left\langle P_{(\alpha)}, P_{(\beta)} \right\rangle_{L_2} = \iint\limits_{u^2+v^2\leq1} P_{(\alpha)} P^*_{(\beta)}\, du\, dv = Q_{(\alpha)}\delta_{\alpha\beta} \tag{12}$$

where $P_{(\alpha)}$ and $P_{(\beta)}$ are two arbitrary polynomials of the set, $P^*_{(\beta)}$ is the complex conjugate of $P_{(\beta)}$, and $\delta_{\alpha\beta}$ is the Kronecker delta function. Additionally, $Q_{(\alpha)}$ is the normalization coefficient and may be computed as [16]

$$Q_{nm} = \frac{\pi}{n+1} \tag{13}$$

B. Zernike Moments for a Continuous 2D Signal

Zernike moments are formed by using the Zernike polynomials from Eq. 3 as the basis functions in the 2D moment equation (Eq. 2). We express such a moment as

$$Z_{nm} = \frac{1}{Q_{nm}} \iint\limits_{u^2+v^2\leq 1} P_{nm}(u,v)\ f(u,v)\ \mathrm{d}u\ \mathrm{d}v \tag{14}$$

although we often find that scaling with the normalization coefficient is not required,

$$A_{nm} = \iint\limits_{u^2+v^2\leq 1} P_{nm}(u,v)\ f(u,v)\ \mathrm{d}u\ \mathrm{d}v, \tag{15}$$

This, of course, leads to the simple scaling relation

$$Z_{nm} = A_{nm}/Q_{nm} \tag{16}$$

C. Rotational Properties of Zernike Moments

Zernike moments of repetition $m = 0$ are rotationally invariant, as the value of the moment A_{nm} is unaffected by the orientation of the underlying signal relative to the $\bar{u}$-$\bar{v}$ coordinate system. For other values of m (i.e., for $m > 0$), we find that the moment A_{nm} changes as the orientation of the underlying signal changes.

Consider, for example, the moment A_{nm} for a particular image patch as computed in the $\bar{u}$-$\bar{v}$ frame. Now consider the moment A'_{nm} for this same image patch as computed in the $\bar{u}'$-$\bar{v}'$ frame that has been rotated by an angle ψ relative to the unprimed frame (see Fig. 1). Noting that $\theta' = \theta - \psi$, it is clear from Eqs. 3 and 15 that

$$A'_{nm} = A_{nm} \exp(-jm\psi) \tag{17}$$

It is this relation that will ultimately allow us to determine the orientation of an edge or line from the moment A_{11}.

D. Zernike Moments for a Digital Image

A digital image, $I(u,v)$, is a quantized representation of the continuous signal $f(u,v)$. The image $I(u,v)$ is presumed to be an array of digital numbers, with integer intensity values (e.g., 0–65,535 for a 16-bit image) occurring at integer values of u and v.

In this case, we approximate the Zernike moment integral from Eq. 15 with a double summation. Therefore, assuming a local image patch of size $N \times N$ centered at a pixel-level edge/line guess of $\{\tilde{u}_i, \tilde{v}_i\}$, one may compute the moment as

$$A_{nm}(\tilde{u}_i, \tilde{v}_i) \approx \sum_{k=-p}^{p} \sum_{s=-p}^{p} I(\tilde{u}_i + s, \tilde{v}_i + k) M_{nm}(p+s, p+k) \tag{18}$$

where $p = (N-1)/2$ is a non-negative integer (since N is an odd integer greater than one). The mask M_{nm} is an $N \times N$ matrix of values found by the integration of P_{nm} over the corresponding pixel and within the patch's inscribed circle. Values of M_{11} and M_{20} are shown for a 5×5 and 7×7 mask in [8]. It is observed that Eq. 18 is simply an image correlation, such that one may compute the moment everywhere in the image according to

$$A_{nm} = M_{nm} * I \tag{19}$$

where $*$ is the 2D correlation operator.

The edge and line localization methods presented here will ultimately only use the moments A_{11} and A_{20}. Of note is that M_{20} is real valued such that

$$A_{20} = M_{20} * I \tag{20}$$

We observe, however, that M_{11} is complex valued,

$$M_{nm} = \mathrm{Re}\left[M_{11}\right] + j\,\mathrm{Im}\left[M_{11}\right] \tag{21}$$

Fortunately, given the structure of M_{11}, one only needs to keep track of the real component in practice since [8]

$$\mathrm{Re}\left[A_{11}\right] = \mathrm{Re}\left[M_{11}\right] * I \tag{22}$$

$$\mathrm{Im}\left[A_{11}\right] = \mathrm{Re}\left[M_{11}\right]^T * I \tag{23}$$

Thus, we may compute all the necessary moments through three simple image correlations (which, in practice, only need to be computed at the pixel-level edge or line locations and not at every point in the image).

IV. Moment-Based Edge and Line Localization

The same procedure may be used for both edge and line localization. In both cases, the image data in a small $N_p \times N_p$ image patch around a pixel-level edge/line guess is scaled according to Eq. 1 and the Zernike moments A_{11} and A_{20} are computed (Eqs. 20, 22, 23). These moments are used to compute the edge/line orientation (ψ) and the distance along this direction by which the pixel-level edge/line guess should be adjusted (ℓ). Consequently, both the edge and the line are corrected to subpixel accuracy by

$$\begin{bmatrix} \bar{u} \\ \bar{v} \end{bmatrix} = \ell \begin{bmatrix} \cos\psi \\ \sin\psi \end{bmatrix} \tag{24}$$

which, after rearranging Eq. 1, yields the correction we seek in practice

$$\begin{bmatrix} u \\ v \end{bmatrix} = \begin{bmatrix} \tilde{u} \\ \tilde{v} \end{bmatrix} + \frac{N_p\,\ell}{2} \begin{bmatrix} \cos\psi \\ \sin\psi \end{bmatrix} \tag{25}$$

The orientation ψ of both edges and lines is found in the same way and using the same equation. The difference between the correction between the edge and line is simply how the Zernike moments are used to compute ℓ.

A. Computing Edge or Line Orientation

Determining the normal direction to an edge or line is achieved in the exact same manner, with the final equation being equivalent for both. By construction, and as can be seen from Fig. 1, the intensity value is only a function of $\bar{u}'$ (i.e., not a function of $\bar{v}'$) for both the edge and the line. We see immediately from the form of P_{11} in Eq. 7 that

$$\mathrm{Im}\left[A'_{11}\right] = 0 \tag{26}$$

Thus, recalling that $\exp(-jm\psi) = \cos(m\psi) - j\sin(m\psi)$, we may rewrite Eq. 17 as (for $m = n = 1$)

$$A'_{11} = A_{11}\left[\cos(\psi) - j\sin(\psi)\right] \tag{27}$$

such that

$$\mathrm{Re}[A'_{11}] = \mathrm{Re}[A_{11}]\cos(\psi) + \mathrm{Im}[A_{11}]\sin(\psi) \tag{28}$$

$$\mathrm{Im}[A'_{11}] = \mathrm{Im}[A_{11}]\cos(\psi) - \mathrm{Re}[A_{11}]\sin(\psi) = 0 \tag{29}$$

The line orientation may be found using the equation for the imaginary component of A'_{nm}. Observing that

$$\mathrm{Im}[A_{11}]\cos(\psi) = \mathrm{Re}[A_{11}]\sin(\psi) \tag{30}$$

we find that the orientation of the line is computed in terms of the moment A_{11} (computed using Eq. 17 and Eq. 30) as

$$\psi = \mathrm{atan2}\left(\mathrm{Im}[A_{11}],\, \mathrm{Re}[A_{11}]\right) \tag{31}$$

This relation has been known for some time for edges [8], [9]. Although obvious within the present framework, this represents the first extension of Eq. 31 to lines (of which the authors are aware).

B. Computing ℓ for Edges

An edge is generally understood to describe a discontinuity in image intensity in one direction, with little intensity change in the direction orthogonal to this discontinuity. Real grayscale images, however, rarely exhibit a true intensity discontinuities. Instead, image blur and pixel quantization cause the intensity change rapidly over a small distance (a few pixels). Thus, we seek areas of high intensity gradient rather than true discontinuities. It has long been known [4] that using a step function for the edge model within a moment-based subpixel edge localization algorithm produces a biased edge update if the image is blurred. This was one of the motivations for introducing a ramp edge model in [8].

In many practical image processing problems, the point spread function (PSF) due to camera defocus and other optical effects is well modeled as a 2D Gaussian [17]. Consequently, the line associated with a crisp edge (a true discontinuity) may be blurred according to

$$I_{blur} \approx K_G * I \tag{32}$$

where I is the perfectly crisp image, K_G is the Gaussian kernel, and I_{blur} is the blurred image. The one-dimensional intensity profile taken perpendicular to the edge is sometimes referred to as the edge spread function (ESF), which will generally take the shape of a sigmoid function. To avoid the mathematical complexities of the sigmoid function within the Zernike moment integrals, it was observed in [8] that a linear ramp provides an adequate engineering approximation for most practical cases. The objective, therefore, is to relate the width of the linear ramp (w, see Fig. 2) with the width of the Gaussian kernel approximating the camera PSF (σ). We do this using the linear relationship

$$w \approx k_{edge}\sigma \tag{33}$$

where k_{edge} is the scaling we seek. In [8], it was suggested to select $k_{edge} = 1.66$. We performed a more comprehensive study and found that choosing $k_{edge} = 1.8$ produced superior performance, especially as the SNR became very large. In general, we found reduced sensitivity to the choice of k_{edge} as the images became noisier (lower SNR).

Therefore, we choose to model an edge as a ramp, whose intensity changes linearly between a background intensity (h) and a foreground intensity ($h + k$). The midpoint of this transition is defined to occur at a distance ℓ from the image patch center and has a width of $2w$. Since we are using Zernike moments, we define all these quantities within the unit disk (Fig. 2). By choosing to define the edge in the $\bar{u}'$-$\bar{v}'$ frame, it is straightforward to write the intensity as a function of $\bar{u}'$ only,

$$I_{edge}(\bar{u}', \bar{v}') = \begin{cases} h & \bar{u}' \le \ell - w \\ h + k\frac{\bar{u}' - (\ell - w)}{2w} & \ell - w < \bar{u}' \le \ell + w \\ h + k & \ell + w < \bar{u}' \end{cases} \tag{34}$$

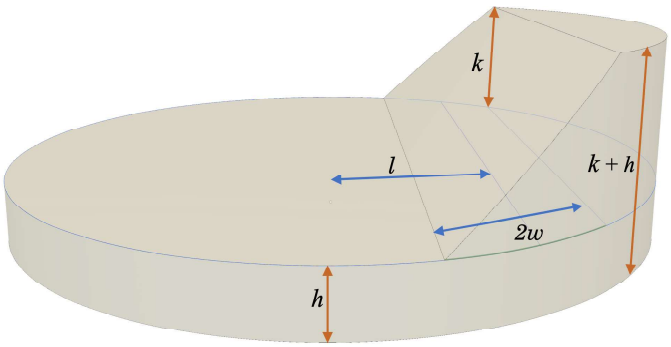

Fig. 2. Graphical representation of an edge on an image within the unit circle, including background intensity h, peak intensity of edge k, edge width w, and distance from the origin to the midpoint of the edge ℓ.

Using this ramp edge model, it is possible to analytically solve the double integral in the moment equation from Eq. 15 in the edge-aligned (i.e., primed) frame. We do this for the moments A'_{11} and A'_{20}, leading to

$$\begin{aligned} A'_{11} = \frac{k}{24w}\Big[&3\arcsin\ell_2 + (3 + 2B_2)\ell_2 B_2 \\ &-3\arcsin\ell_1 - (3 + 2B_1)\ell_1 B_1\Big] \end{aligned} \tag{35}$$

$$A'_{20} = A_{20} = \frac{k}{15w}\left[B_1^5 - B_2^5\right] \tag{36}$$

where

$$\ell_1 = \ell - w \quad \text{and} \quad \ell_2 = \ell + w \tag{37}$$

and

$$B_1 = \sqrt{1 - \ell_1^2} \quad \text{and} \quad B_2 = \sqrt{1 - \ell_2^2} \tag{38}$$

Looking at the expressions for A'_{11} and A'_{20}, it is immediately evident that the the intensity-dependent variable k (which describes the magnitude of the intensity change across the edge) cancels out if one considers the ratio, Q_E

$$Q_E = \frac{A'_{20}}{A'_{11}} = \frac{A_{20}}{A'_{11}} \tag{39}$$

In many cases the edge width w is known (e.g., from the imaging system point spread function), such that Q_E is a function of only ℓ. Although the analytic expression for Q_E is rather cumbersome, it was found in [8] that

$$Q_E \approx \ell\Big[1-(1+\ell/2)w^2\Big] \tag{40}$$

which may be rearranged to solve for the unknown ℓ

$$\hat{\ell}_E \approx \frac{1-w^2-\sqrt{(w^2-1)^2-2w^2Q_E}}{w^2} \tag{41}$$

C. Computing ℓ for Lines

As a natural extension to the ideal step-function ESF, we model the ideal line spread function (LSF) as an impulse (where the LSF is defined as the 1D intensity profile perpendicular to the line). As before, the perfectly crisp image is blurred with a Gaussian kernel, thus spreading out the line intensity—with the resulting LSF being Gaussian PDF. Rather than deal with the mathematical complexities of the Gaussian PDF, we choose to model the line PSF as a wedge. To make practical use of the wedge model, it is necessary to determine the relationship between the wedge width (w, see Fig. 3) and the Gaussian kernel width (σ),

$$w \approx k_{line}\sigma \tag{42}$$

where k_{line} is the parameter we seek. We found that choosing $k_{line} = 0.9$ provided the best results, with low SNR images exhibiting less sensitivity to the exact choice of this parameter.

The small image patch centered about the pixel-level guess is assumed to have a constant background intensity of h and contain a line of intensity $h+k$. The wedge has a full width of $2w$ with a peak intensity occurring at a distance ℓ from the image patch (or disk) center. The sides of the wedge are linear ramps transitioning between the background and the line's ridgeline. This is shown pictorially on the unit disk in Fig. 3.

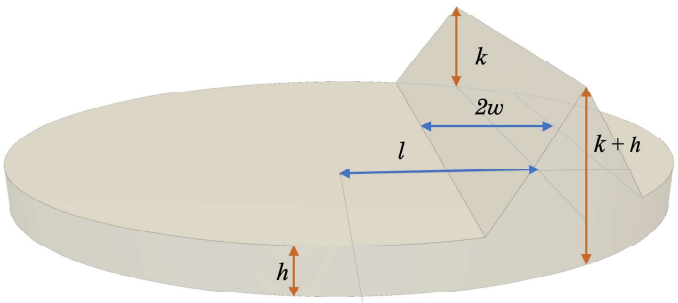

Fig. 3. Graphical representation of a line on an image within the unit circle, including background intensity h, peak intensity of line k, width of the line w, and distance from the origin to the line ℓ.

As with the edge, we choose to define the line model in the $\bar{u}'$-$\bar{v}'$ frame such that the intensity is a function of $\bar{u}'$ only (and not a function of $\bar{v}'$),

$$I_{line}(\bar{u}',\bar{v}') = \begin{cases} h & \bar{u}' \le \ell - w \\ h + k\frac{\bar{u}'-(\ell-w)}{w} & \ell - w < \bar{u}' \le \ell \\ h + k - k\frac{\bar{u}'-\ell}{w} & \ell < \bar{u}' \le \ell + w \\ h & \ell + w < \bar{u}' \end{cases} \tag{43}$$

The analytical value of A'_{11} and A'_{20} may be found by evaluating the double integral from Eq. 15

$$\begin{aligned} A'_{11} = \frac{k}{12w}\Big[&6\arcsin\ell - 3\arcsin\ell_1 - 3\arcsin\ell_2 \\ &+2\ell C(5-2\ell^2) \\ &-\ell_1 B_1(3+2B_1^2) \\ &-\ell_2 B_2(3+2B_2^2)\Big] \end{aligned} \tag{44}$$

and

$$A'_{20} = \frac{2k}{15w}\Big[B_1^5 + B_2^5 - 2C^5\Big], \tag{45}$$

where B_1 and B_2 are from Eq. 38 and

$$C = \sqrt{1-\ell^2} \tag{46}$$

The ratio of A'_{20} to A'_{11} eliminates k, thus providing a function of only ℓ and w,

$$Q_L(\ell, w) = \frac{A'_{20}}{A'_{11}} = \frac{A_{20}}{A'_{11}} \tag{47}$$

Assuming the line width w is known, we seek to rearrange Q_L to solve for the unknown ℓ. The complicated form of Q_L after substitution of Eq. 44 and Eq. 45 makes finding an analytic solution difficult for arbitrary values of w and ℓ. Fortunately, it is straightforward to find an approximation that is good enough for most practical image processing applications.

We know that lines are thin, so it is instructive to explore what happens to Q_L as $w \to 0$. We find that the limit does permit a simple analytic solution,

$$Q_{L_0} = \lim_{w\to 0} Q_L = \frac{4\ell_{L_0}^2 - 1}{3\ell_{L_0}} \tag{48}$$

which may be solved for for ℓ_{L_0}

$$\hat{\ell}_{L_0} = \frac{3}{8}Q_{L_0} \pm \sqrt{\left(\frac{3}{8}Q_{L_0}\right)^2 + \frac{1}{4}} \tag{49}$$

To choose the correct root, observe that

$$\lim_{\ell_{L_0}\to 0^+} Q_{L_0} = \lim_{\ell_{L_0}\to 0^+} \frac{4\ell_0^2 - 1}{3\ell_0} = -\infty \tag{50}$$

where we know to choose the right limit since $\ell_L \ge 0$ by construction. Thus we seek the root that is approximately zero when Q_{L_0} is a large negative number, which only happens when the plus sign is chosen in Eq. 49. Therefore,

$$\hat{\ell}_{L_0} = \frac{3}{8}Q_{L_0} + \sqrt{\left(\frac{3}{8}Q_{L_0}\right)^2 + \frac{1}{4}} \tag{51}$$

This analytic result may be generalized to the situation where $w > 0$, which does not appear to permit an exact analytic solution. Therefore, we write a parameterized expression for ℓ_L that simplifies exactly to Eq. 51 when $w = 0$ and fit the parameters in a least squares sense. Using this approach, consider a model of the form

$$\hat{\ell}_L \approx \sqrt{a_1^2 Q_L^2 + a_2 Q_L w + a_3 w^2 + a_4 w + a_5} + a_6 Q_L + a_7 w + a_8 \tag{52}$$

We found the terms associated with a_1, a_3, a_5, and a_6 to dominate the estimate of ℓ_L, with the remaining terms contributing relatively little. Furthermore, it was found that $a_1 \approx a_6$ regardless of the test set-up. Therefore, discarding the unimportant terms and letting $a_1 = a_6$, we performed a three parameter fit for the line correction of the form

$$\hat{\ell}_L \approx \sqrt{a_1^2 Q_L^2 + a_3 w^2 + a_5} + a_1 Q_L. \tag{53}$$

The result of the least squares fit found the values of a_1 and a_5 to exactly match the analytically derived coefficients for ℓ_{L_0} in Eq. 51

$$a_1 = 3/8, \quad a_5 = 1/4 \tag{54}$$

and empirically found that

$$a_3 \approx -1/10 \tag{55}$$

Therefore, we may write the empirically derived expression for the line update for arbitrary w as

$$\hat{\ell}_L = \frac{3}{8} Q_L + \sqrt{\left(\frac{3}{8} Q_L\right)^2 - \frac{1}{10} w^2 + \frac{1}{4}} \tag{56}$$

V. Numerical Validation on Synthetic Images

The performance of the edge and line localization methods presented in this work were quantitatively evaluated using synthetic images. We find synthetic images to be especially useful in this context since the true continuous location of every image feature is known. The perfectly known continuous underlying signal may be blurred to simulate camera defocus and quantized (both spatially and in intensity) to simulate differing image resolutions. Further, noise may be added with a prescribed intensity, allowing the unambiguous evaluation of performance as a function of signal-to-noise ratio (SNR). This is important, as the localization of edges is known to become more challenging as SNR decreases [18].

For the examples presented here, perfect images were blurred by using a Gaussian point spread function (PSF). After blurring, zero-mean Gaussian noise was added to achieve the specified SNR.

A. Synthetic Images with Edges

1) Ideal Edge Localization Performance

It is important to quantify the error associated with the approximations used to arrive at the analytic edge update given in Eq. 41. Therefore, as a bounding case, suppose that we perfectly compute the Zernike moments for a noise-free continuous signal. In this situation, the error in $\hat{\ell}_E$ is given by the contours in Fig. 4 for different situations. These contours make clear the performance improvement realized by switching form the step-function edge model (red contours) to the ramp edge model (black contours). The results shown here are identical to the observations of Christian in [8].

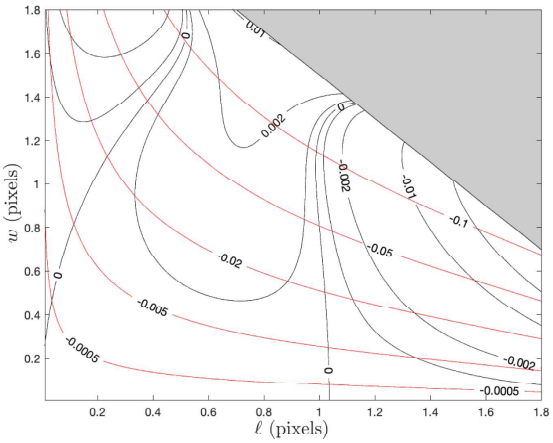

Fig. 4. Contours of edge localization error for a continuous (not pixelated) ramp edge signal. Black contours show the error when using the approximation from Eq. 41, red contours show the error when using the step function approximation from [9].

2) Digital Image Edge Localization Performance

Our method performed favorably to other existing techniques when processing synthetic digital imagery. This was assessed through a Monte Carlo analysis where we evaluated performance of different algorithms for images having varying amounts of blur and noise. Figure 5 shows edge localization error with our technique (black contours) compared against the moment-based solution with a step-function edge model [9] and the partial area effect (PAE) [6]. Results for both of the two moment-based methods shown here assume a 5×5 pixel mask.

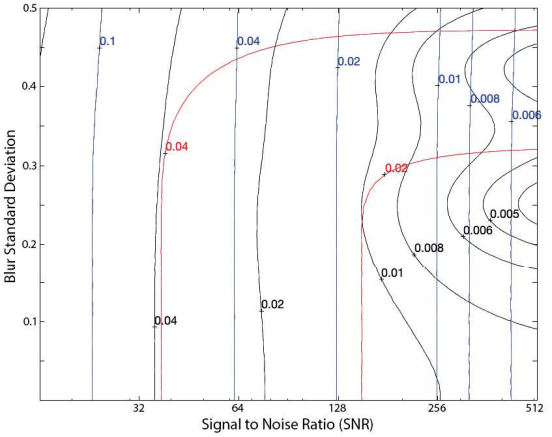

Fig. 5. Contours of edge localization error (in pixels, assuming a 5×5 mask) for our method (black), the step function approximation using Zernike moments (red) [9], and the partial area effect (blue) [6] as a function of SNR and blur levels.

We observe that the PAE algorithm produced nearly perfect edge localization in cases with no noise (infinite SNR; off the right-hand side of Fig 5). The Zernike moment methods tended to perform better than the PAE method as noise increased (as SNR decreased; towards the left-hand side of Fig 5). The method presented in this work outperforms the PAE method for most real-life SNR values.

Example performance of our subpixel edge localization algorithm in different noise/blur cases is shown in Fig. 6. This example shows localization of the edge of a circle. Clear improvement is evident in all cases, as the algorithm moves the pixel-level edge guess (red $\times$) towards the true edge location (black line). We know the true edge location since these are synthetic images.

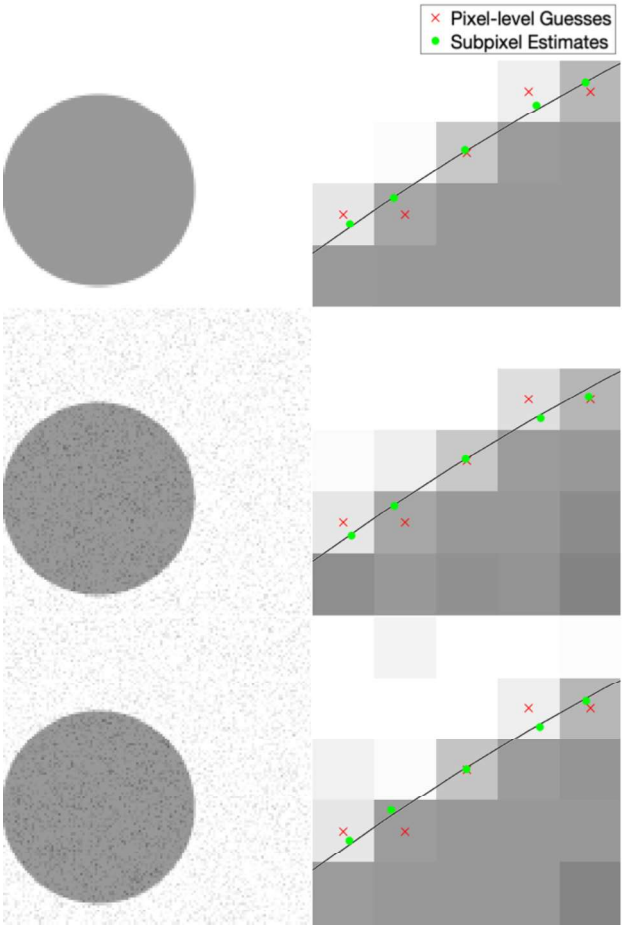

Fig. 6. Qualitative visualization of subpixel edge localization performance at varying levels of blur and SNR. The left column shows the full synthetically generated image and the right column shows a small area within that image. The rows represent different noise and blur levels (top: no noise or blur; middle: noise only; bottom: noise and blur). The black line is the exact location of the true edge.

B. Synthetic Images with Lines

1) Ideal Line Localization Performance

As with the case of edges, we begin the numerical assessment of our subpixel line localization method by considering the case of a continuous signal. This allows us to directly quantify the error associated with the approximations used to arrive at the analytic expression in Eq 56. We considered all reasonably plausible combinations of line location (ℓ) and line width (w) and produced contours of errors in the estimate $\hat{\ell}_L$, as shown in Fig. 7. These errors low enough to be negligible when applied to a pixelated image.

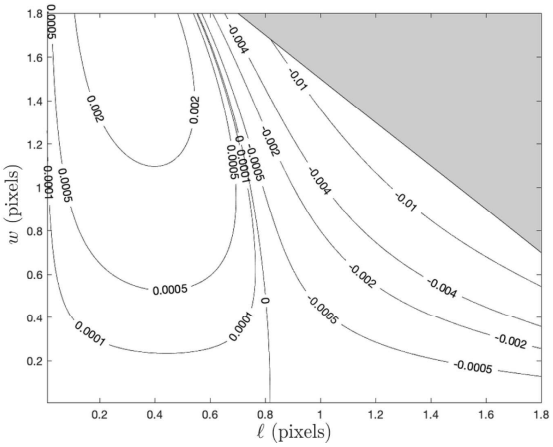

Fig. 7. Contours of line localization error when using Eq. 56 for a continuous (not pixelated) wedge edge signal.

2) Digital Image Line Localization Performance

Our Zernike moment method also performed well in the subpixel localization of lines. We performed a Monte Carlo analysis where line localization error was recorded for varying amounts of image blur and noise. The results are shown as contours in Fig. 8. As expected, localization performance decreases with increased noise and blur.

Example performance of our subpixel line localization algorithm in different noise/blur cases is shown in Fig. 9. This example shows localization of a circular line. Clear improvement is evident in all cases, as the algorithm moves the pixel-level line guess (red $\times$) towards the true line location (black line). We know the true line location since these are synthetic images.

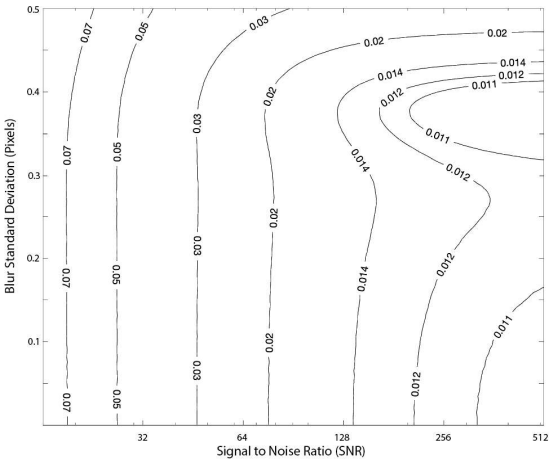

Fig. 8. Contours of line localization error (in pixels, assuming a 5×5 mask) for our method as a function of SNR and blur levels.

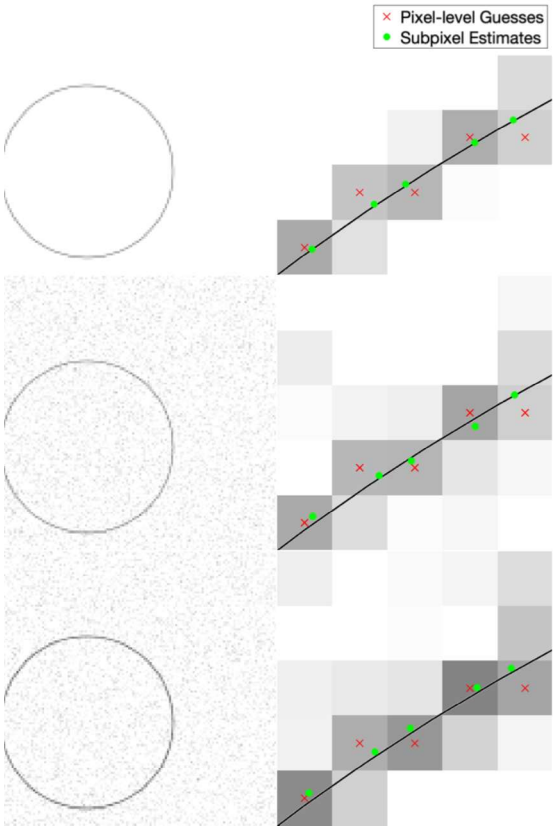

Fig. 9. Qualitative visualization of subpixel line localization performance at varying levels of blur and SNR. The left column shows the full synthetically generated image and the right column shows a small area within that image. The rows represent different noise and blur levels (top: no noise or blur; middle: noise only; bottom: noise and blur). The black line is the exact location of the true line center.

VI. Validation on real data

After confirming that estimate edge and line locations agree with the truth in simulated images, we apply our method to real digital images. As these real-world images do not provide perfect subpixel knowledge of the edge or line location, verifying results is from visual inspection and is largely qualitative.

It is important to remember that the algorithm presented here only performs the subpixel localization (i.e., correction) on pixel-level location guesses (e.g., using Sobel [1], Canny [3], or other method); any lines that the higher-level algorithm fails to identify will not contribute to the final result. Note that these pixel-level guesses may be found automatically or manually. Regardless of how they are found, the subpixel correction is automatic.

This section includes a number of example images with the accompanying results from the methods proposed in this paper. These examples show the raw image on the left-most frame, followed by two sections of the image in grayscale containing lines or edges of interest (center and right frame). The middle frame of each example only shows the subpixel estimate overlay (green dots). The right frame of each example shows both the pixel-level guess (red $\times$) and the subpixel estimate (green dots) overlay. The right frame also shows the edge or line estimates connected by a line to highlight the improvement in smoothness automatically produced by the subpixel correction.

Figure 10 shows an application to satellite imagery that illustrates the difference in the shores of the Mississippi River in the aftermath of a flood (top) and its normal banks (bottom). Figures 11, 12, and 13 show various space images to which we have applied this technique. Figure 14 traces the routes of blood vessels in a retinal scan to highlight the potential use of this method in medical imaging.

VII. Conclusion

Zernike moments are powerful tools in image processing. Correcting a pixel-level guess of either an edge or a line requires use of only two moments: A_{11} and A_{20}. We show that it is possible to accurately locate both edges and lines using an analytic function of these two moments. Furthermore, this method is tolerant to noise and outperforms other existing methods. Performance was quantitatively evaluated on synthetic images (better than 0.1 pixels for both edges and lines) and qualitatively evaluated on real images. Applications were shown to remote sensing, space exploration, and medical imaging.

VIII. Acknowledgements

The authors are thankful to Huntington Gazecki who assisted with early work on this topic during his time as an undergraduate student at RPI. This work was made possible by the Air Force Office of Scientific Research (AFOSR) through award FA9550-16-1-0234.

References

[1] I. Sobel, "An isotropic 3x3 image gradient operator," *Presentation at Stanford A.I. Project 1968*, 02 2014.

[2] D. Marr and E. Hildreth, "Theory of edge detection," *Proceedings of the Royal Society of London. Series B, Biological Sciences*, vol. 207, no. 1167, pp. 187–217, 1980.

[3] J. F. Canny, "A computational approach to edge detection," *IEEE Transactions on Pattern Analysis and Machine Intelligence*, vol. PAMI-8, pp. 679–698, 1986.

[4] E. P. Lyvers, O. R. Mitchell, M. L. Akey, and A. P. Reeves, "Subpixel measurements using a moment-based edge operator," *IEEE Transactions on Pattern Analysis and Machine Intelligence*, vol. 11, no. 12, pp. 1293–1309, Dec 1989.

[5] J. Ye, G. Fu, and U. Poudel, "High-accuracy edge detection with Blurred Edge Model," *Image and Vision Computing*, vol. 23, pp. 453–467, 2005.

[6] A. Trujillo-Pino, K. Krissian, M. Alemn-Flores, and D. Santana-Cedrs, "Accurate subpixel edge location based on partial area effect," *Image and Vision Computing*, vol. 31, no. 1, pp. 72 – 90, 2013.

[7] T. Hermosilla, E. Bermejo, A. Balaguer, and L. Ruiz, "Non-linear fourth-order image interpolation for subpixel edge detection and localization," *Image and Vision Computing*, vol. 26, pp. 1240–1248, 2008.

[8] J. A. Christian, "Accurate planetary limb localization for image-based spacecraft navigation," *Journal of Spacecraft and Rockets*, vol. 54, no. 3, pp. 708–730, 2019/02/14 2017.

[9] S. Ghosal and R. Mehrotra, "Orthogonal moment operators for subpixel edge detection," *Pattern Recognition*, vol. 26, no. 2, pp. 295 – 306, 1993.

[10] A. B. Bhatia and E. Wolf, "On the circle polynomials of zernike and related orthogonal sets," *Mathematical Proceedings of the Cambridge Philosophical Society*, vol. 50, no. 1, p. 4048, 1954.

[11] F. von Zernike, "Beugungstheorie des schneidenver-fahrens und seiner verbesserten form, der phasenkontrastmethode," *Physica*, vol. 1, no. 7, pp. 689 – 704, 1934.

[12] A. Khotanzad and Y. H. Hong, "Invariant image recognition by zernike moments," *IEEE Transactions on Pattern Analysis and Machine Intelligence*, vol. 12, no. 5, pp. 489–497, May 1990.

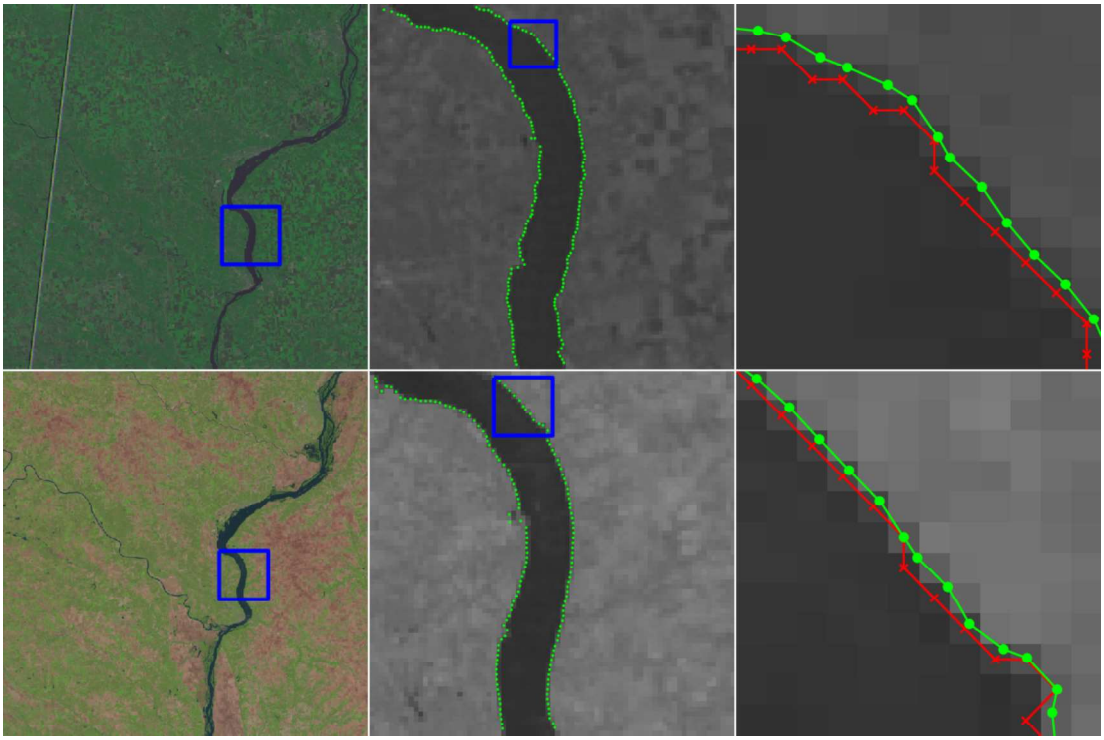

Fig. 10. Images of the Mississippi River taken by the Landsat-5 spacecraft. The top image (LM05 L1TP_025032_20120830_20180521_01_T2) was collected on 21 May 2018 by the Multispectral Scanner System (MSS) and shows the river during normal conditions. The bottom image (LT05_L1TP_025032 20110508_20160902_01_T1) was collected on 2 September 2011 by the Thematic Mapper (TM) and shows the river after a major flooding event. The red $\times$ symbols denote pixel-level edge estimates, and green dots denote the refined subpixel localization estimates. Image data is available from the U.S. Geological Survey (USGS) [19].

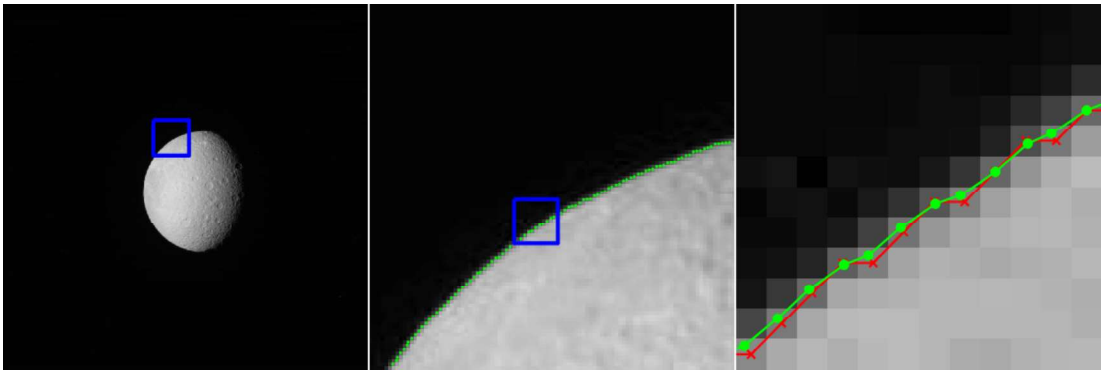

Fig. 11. Image of Rhea (a moon of Saturn) collected by the Cassini spacecrafts Narrow Angle Camera (NAC) on 13 October 2006 (raw image N1539252663 [20]). The red $\times$ symbols denote pixel-level edge estimates, and green dots denote the refined subpixel localization estimates.

[13] T.-W. Lin and Y.-F. Chou, "A comparative study of zernike moments," in *Proceedings IEEE/WIC International Conference on Web Intelligence (WI 2003)*, Oct 2003, pp. 516–519.

[14] C. . Teh and R. T. Chin, "On image analysis by the methods of moments," *IEEE Transactions on Pattern Analysis and Machine Intelligence*, vol. 10, no. 4, pp. 496–513, July 1988.

[15] W. Tango, "The circle polynomials of zernike and their application in optics." *Applied Physics*, vol. 13, no. 4, p. 327, 1977.

[16] M. Born and E. Wolf, *Principles of optics : electromagnetic theory of propagation, interference and diffraction of light.* Cambridge, UK ; New York : Cambridge University Press, 1997., 1997.

[17] U. V. G. Rao and V. K. Jain, "Gaussian and exponential approximations of the modulation transfer function," *J. Opt. Soc. Am.*, vol. 57, no. 9, pp. 1159–1160, Sep 1967.

[18] N. Ofir, M. Galun, S. Alpert, A. Brandt, B. Nadler, and R. Basri, "On detection of faint edges in noisy images," *IEEE transactions on pattern analysis and machine intelligence*, 2019.

[19] EarthExplorer. Earth Resources Observation and Science (EROS) Center, U.S. Geological Survey (USGS). [Online]. Available: https://earthexplorer.usgs.gov

[20] C. Porco, "CASSINI ORBITER SATURN ISSNA/ISSWA 2 EDR VERSION 1.0," 2005.

[21] NASA, Johns Hopkins University Applied Physics Laboratory, & Southwest Research Institute, "New Horizons LORRI Images," 2019.

[22] A. Hoover, V. Kouznetsova, and M. Goldbaum, "Locating blood vessels in retinal images by piece-wise threhsold probing of a matched filter response," *IEEE Transactions on Medical Imaging*, vol. 19, no. 3, pp. 203–210, 2000.

[23] A. Hoover and M. Goldbaum, "Locating the optic nerve in a retinal image using the fuzzy convergence of the blood vessels," *IEEE Transactions on Medical Imaging*, vol. 22, no. 8, pp. 951–958, 2003.

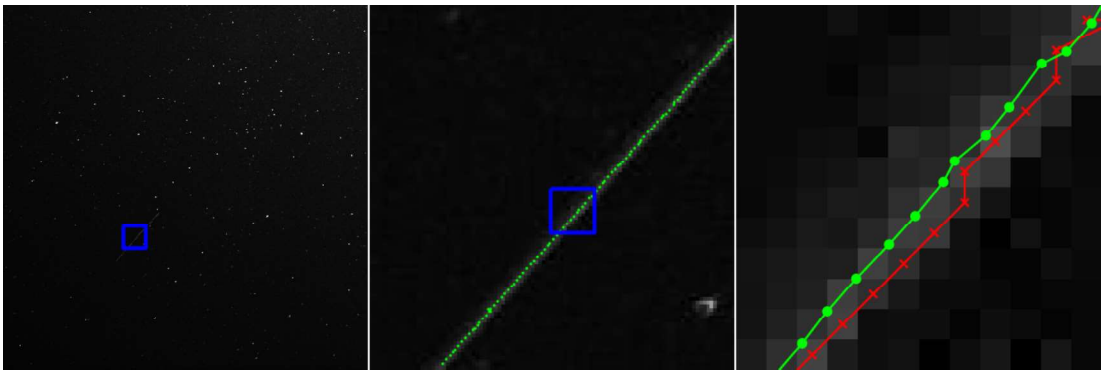

Fig. 12. Inertially pointed star field image captured with with the Omnidirectional Space Situational Awareness (OmniSSA) system. This example image has a 10 second exposure time and contains a satellite that appears as a streak (line) within the image. The red $\times$ symbols denote pixel-level line estimates, and green dots denote the refined subpixel localization estimates. The original OmniSSA image is courtesy of Dr. Marcus Holzinger of University of Colorado Boulder.

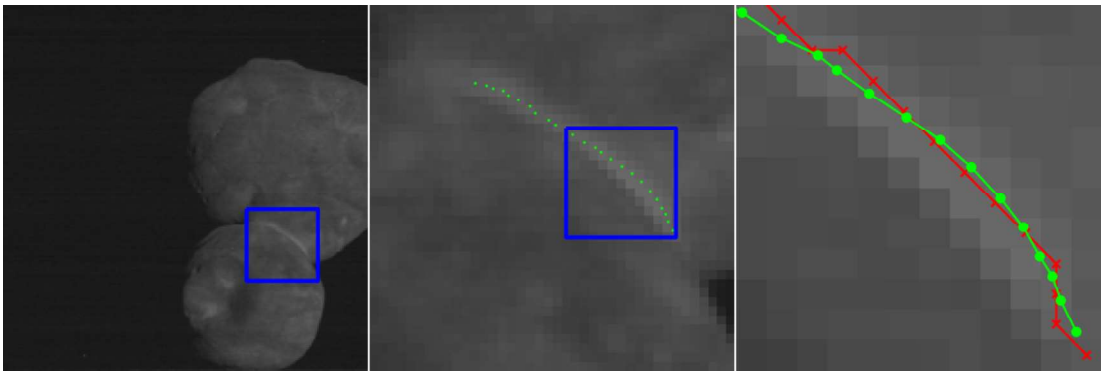

Fig. 13. New Horizon's Long Range Reconnaissance Imager (LORRI) captured this image of Kuiper belt object Arrokoth (formerly called Ultima Thule) during a flyby in early 2019 [21]. The red $\times$ symbols denote pixel-level line estimates, and green dots denote the refined subpixel localization estimates.

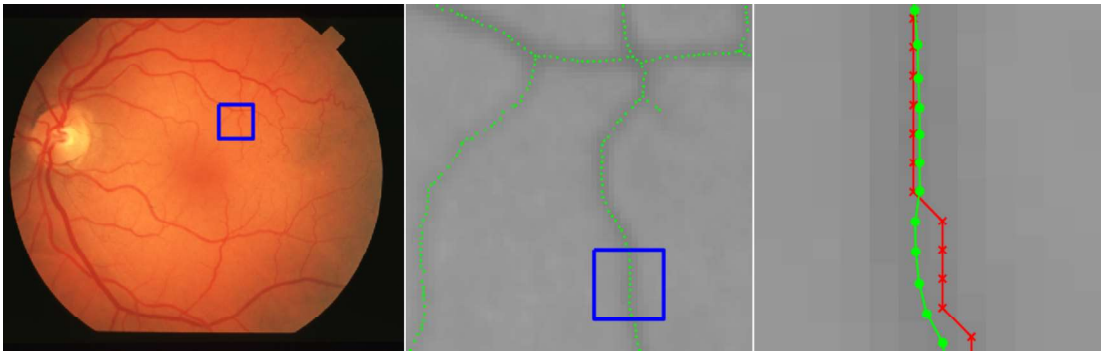

Fig. 14. Image of a retinal scan for a healthy eye, where we seek to localize blood vessels. The red $\times$ symbols denote pixel-level edge estimates, and green dots denote the refined subpixel localization estimates. The original image is im00032 from the STARE database [22], [23].

Chapter 6

Appendix B - Journal Publications